# Winter snow cover on the sea ice of the Arctic Ocean at the Surface Heat Budget of the Arctic Ocean (SHEBA): Temporal evolution and spatial variability

Matthew Sturm and Jon Holmgren
U.S. Army Cold Regions Research and Engineering Laboratory – Alaska, Ft. Wainwright, Alaska, USA

Don K. Perovich
U.S. Army Cold Regions Research and Engineering Laboratory, Hanover, New Hampshire, USA

Received 1 May 2000; revised 12 January 2001; accepted 23 July 2001; published 25 October 2002.

[1] The evolution and spatial distribution of the snow cover on the sea ice of the Arctic Ocean was observed during the Surface Heat Budget of the Arctic Ocean (SHEBA) project. The snow cover built up in October and November, reached near maximum depth by mid-December, then remained relatively unchanged until snowmelt. Ten layers were deposited, the result of a similar number of weather events. Two basic types of snow were present: depth hoar and wind slab. The depth hoar, 37% of the pack, was produced by the extreme temperature gradients imposed on the snow. The wind slabs, 42% of the snowpack, were the result of two storms in which there was simultaneous snow and high winds (>10 m $s^{-1}$). The slabs impacted virtually all bulk snow properties emphasizing the importance of episodic events in snowpack development. The mean snow depth ($n$ = 21,169) was 33.7 cm with a bulk density of 0.34 g $cm^{-3}$ ($n$ = 357, $r^2$ of 0.987), giving an average snow water equivalent of 11.6 cm, 25% higher than the amount record by precipitation gauge. Both depth and stratigraphy varied significantly with ice type, the greatest depth, and the greatest variability in depth occurring on deformed ice (ridges and rubble fields). Across all ice types a persistent structural length in depth variations of ~20 m was found. This appears to be the result of drift features at the snow surface interacting with small-scale ice surface structures. A number of simple ways of representing the complex temporal and spatial variations of the snow cover in ice-ocean-atmosphere models are suggested. *INDEX TERMS:* 1863 Hydrology: Snow and ice (1827); 1827 Hydrology: Glaciology (1863); 4207 Oceanography: General: Arctic and Antarctic oceanography; 4540 Oceanography: Physical: Ice mechanics and air/sea/ice exchange processes; *KEYWORDS:* snow, sea ice, Arctic, SHEBA

**Citation:** Sturm, M., J. Holmgren, and D. K. Perovich, Winter snow cover on the sea ice of the Arctic Ocean at the Surface Heat Budget of the Arctic Ocean (SHEBA): Temporal evolution and spatial variability, *J. Geophys. Res.*, *107*(C10), 8047, doi:10.1029/2000JC000400, 2002.

## 1. Introduction

[2] Snow plays two important but somewhat conflicting roles in the energy balance of the ice-covered Arctic Basin. On one hand, due to its high albedo, it reflects up to 85% of the incoming shortwave solar radiation [*Geiger*, 1957; *Barry*, 1996], significantly retarding melting in the spring. On the other hand, because it is an excellent thermal insulator [*Mellor*, 1964], snow decreases the rate of sensible heat loss from the ocean and ice, a process that promotes slower ice growth. The balance between these two effects is critical in determining the overall heat budget of the Arctic Ocean and the thickness of the sea ice [*Maykut and Untersteiner*, 1971; *Ledley*, 1991].



[3] One of the chief goals of the Surface Heat Budget of the Arctic Ocean (SHEBA) [*Perovich et al.*, 1999a, 1999b] was to understand the full suite of processes governing the exchange of energy between the ocean and the atmosphere in the Arctic Basin. Because of the importance of snow in these exchange processes, a detailed set of measurements of the temporal development and spatial distribution of the snow cover were made during the experiment. They are reported here. Surprisingly, only a few prior descriptions of the Arctic Ocean snow cover are available.

[4] A second goal of SHEBA was to produce improved parameterizations of energy and mass exchange processes for regional and global models. Unfortunately, the snow cover is variable in both in time and space. It builds up as the result of an irregular sequence of precipitation and wind events that are hard to predict. The wind scours the snow from some areas, deposits it in others, leading to large lateral gradients in snow properties including depth, density,

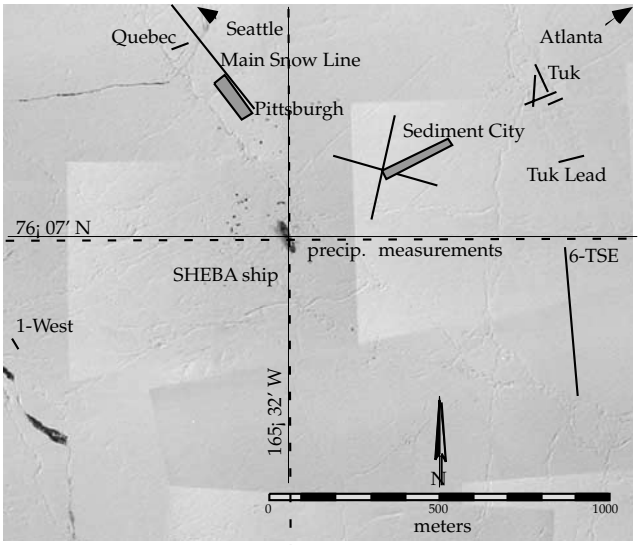


**Figure 1.** Location of the snow measurement stations closest to the SHEBA ship. Lines and boxes indicate measurement probe lines and mapped areas. Stations farther from the camp are listed in Table 1 but are not shown on Figure 1 to allow details of the ice to be visible. Camp position is for 18 April 1998, midway through the intensive snow measurement period; the photomosaic is from 17 May 1998, but little change had occurred in the snow and ice between the two dates.

stratigraphy, and thermal conductivity. Ice thickness, temperature, and surface roughness all play a role in determining the amount of snow initially deposited and its subsequent metamorphism, thereby affecting the albedo, the thermal conductivity, and the snow water equivalence. Modeling the snow cover accurately is not simple. It requires that we understand the spatial and temporal variability of the snow properties. Based on our study, we provide guidance on how this modeling might best be done.

## 2. Methods

[5] Snow observations started in October 1997 when the SHEBA camp was established in the Beaufort Sea at 75°N, 142°W. They were continued until 11 October 1998 when the camp was closed. During that period, the camp drifted 2800 km to 80°N, 162°W. Stake lines (e.g., ''main snow line'' in Figure 1) ranging from 200 to 500 m in length were installed shortly after the camp was established. Snow depth and ice thickness were measured at the stakes and between them 14 to 46 times during the year, with the greater frequency at the lines closer to the ship [*Perovich et al.*, 1999a, 1999b]. An observer would walk along the line, reading the depths on ruled tapes affixed to the stakes, or probing the depth with a pole every few meters between the stakes. About halfway through the year, manual depth measurements with a probe pole were replaced by measurements made using a self-reading probe (available at http://www.uspto.gov/patft/index.html; see patent 5,864,059) which increased the number of readings substantially. This change, and other contributing factors like weather, darkness, and a variety of observers, resulted in a wide range in the spacing, location, and number of measurements on each line. We have made statistical adjustments in order to compare the data between one set of measurements and the next. Break-up of the ice and ridging also resulted in measurements sequences that did not sample the same spatial base, for which corrections have also been made.

[6] Hourly measurements of air temperature, wind speed and direction, humidity, and precipitation were recorded just south of the SHEBA camp (R. Moritz, personal communication, 1999). A sonic depth sounder (Campbell Scientific UDG-01) mounted at the station called ''Seattle'' (Figure 1) recorded the hourly change in the surface elevation of the snow from 1 November 1997 onward and was accurate to ±5 mm. It could also be used to determine when snow transport was taking place because the acoustic signal was degraded during those times. At the time it was put into operation, an average of 11 cm of snow ice and snow covered the sea ice at the site, a small melt pond that had recently refrozen. Hourly readings of temperatures within the ice and snow were also recorded at the Seattle site using thermistors (spaced vertically every 0.1 m) attached to a pole that was placed in a hole drilled into the ice and which extended up into the snow [*Perovich and Elder*, 2001].

[7] Between 28 March and 11 May, a period when the snow cover had reached near maximum depth but had not yet started to melt, intensive measurements of snow depth, density, stratigraphy, snow water equivalent (SWE), and hardness were made at 70 stations located between 0.5 and 16 km from the ship (Figure 1 and Table 1). At most stations a 100 m tape was laid out and the snow depth was probed every 0.5 m. A hole was drilled through the ice and the seawater was used as a datum for a level survey of the snow surface, again at the 0.5 m spacing. A rotating laser and self-reading rod (SmartStik, accurate to ±0.02 m) was used for this purpose, as described by *Holmgren et al.* [1998]. Subtracting snow depth from the snow surface elevation gave the ice surface profile. The snow water equivalent (SWE) was determined at 10 locations along the line using a tube to core through the snow to the ice and then weighting the cores. The stratigraphy was observed and classified in 6 snow pits using techniques described in the International Classification for snow on the Ground [*Colbeck et al.*, 1992], including a qualitative test for snow hardness. Occasionally, a long trench instead of a pit was excavated and the stratigraphy in the trench wall was recorded. Sometimes using a hand probe, other times using an FM-CW radar [*Holmgren et al.*, 1998], snow depths were collected over longer traverse lines (200 to 1000 m) at a spacing of 0.1 m. At four locations, depths were measured at 0.l m intervals on multiple parallel lines spaced 2 m apart in order to map snow depth contours over areas of several hectares (two of these areas are shown in Figure 1).

## 3. Results

### 3.1. Temporal Evolution

[8] The snow cover at SHEBA built up in October and November, achieving relative maturity and near maximum depth by mid-December. From then until late May, its depth and properties changed only a small amount (Figure 2). At sites near ridges, there was a modest secondary increase in depth toward the end of the winter (April–May), but in

**Table 1.** Station List Showing Bearing and Distance From SHEBA Camp and Some Average Station Statistics[a]

| Number | Station | Distance, km | Bearing, degrees | Ice Code | Ice Thickness, m | *n* | Depth, cm | SD, cm | Maximum, cm | Minimum, cm | SWE, cm | SD, cm | Bulk Density, g/cm3 |
|---|---|---|---|---|---|---|---|---|---|---|---|---|---|
| 1 | Atlanta | 1.5 | 65 | 2 | 1.74 | 204 | 28.0 | 11.42 | 55.99 | 8.8 | 13.6 | 6.1 | 0.39 |
| 2 | Atlanta triangle | 2.2 | 60 | 3 | | 201 | 29.2 | 11.9 | 61.3 | 1.5 | 10.2 | 2.6 | 0.31 |
| 3 | Atlanta triangle radar | 2.2 | 60 | 3 | | no data | | | | | 12.1 | 6.4 | 0.35 |
| 4 | Atlanta 12 m trench | 1.5 | 65 | 2 | | 49 | 29.2 | 9.9 | 47.0 | 11.0 | 8.8 | 2.9 | 0.30 |
| 5 | 3 east | 2.8 | 55 | 3 | 1.65 | 120 | 20.1 | 7.1 | 38.6 | 6.9 | 5.5 | 2.0 | 0.30 |
| 6 | 3 east-R1 | 2.8 | 55 | 0 | 1.65 | 201 | 55.9 | 14.9 | 92.1 | 26.7 | | | |
| 7 | 3 east-R2 | 2.8 | 55 | 0 | 1.65 | 201 | 36.1 | 10.9 | 66.5 | 14.1 | | | |
| 8 | 2 east | 4.6 | 35 | 1 | 1.58 | 201 | 36.9 | 16.7 | 80.2 | 1.0 | | | |
| 9 | 1 east | 6.0 | 36 | 1 | | 201 | 11.9 | 5.5 | 28.2 | 3.6 | | | |
| 10 | Tuk13000 | 0.7 | 72 | 0 | | 201 | 30.9 | 15.7 | 80.2 | 0.9 | 16.4 | 12.4 | 0.34 |
| 11 | Tuk14000 | 0.7 | 72 | 4 | | 201 | 61.2 | 27.4 | 109.7 | 6.8 | | | |
| 12 | TukLead | 0.7 | 78 | 0 | 1.5 | 201 | 41.9 | 20.2 | 87.8 | 11.0 | | | |
| 13 | Tuk15000 | 0.7 | 72 | 0 | | 204 | 22.9 | 14.8 | 86.7 | 1.6 | 10.1 | 9.3 | 0.34 |
| 14 | Tuk16000 | 0.7 | 72 | 0 | | 200 | 29.1 | 23.1 | 102.9 | 1.0 | | | |
| 15 | Tuk cross line | 0.7 | 78 | 4 | | 201 | 32.7 | 13.0 | 93.4 | 8.1 | 8.1 | 5.7 | 0.31 |
| 16 | Tuk cross line radar | 0.7 | 78 | 0 | | 201 | 28.2 | 10.7 | 63.6 | 6.3 | | | |
| 17 | 2 NE | 1.5 | 350 | 4 | | 192 | 17.2 | 9.9 | 52.2 | 0.9 | | | |
| 18 | 1 NE (2.55 km 031°) | 2.6 | 31 | 2 | 1.64 | 201 | 21.8 | 5.3 | 40.9 | 6.3 | 5.5 | 1.8 | 0.32 |
| 19 | Seattle | 0.7 | 337 | 2 | 2.4 | 201 | 41.8 | 17.4 | 103.6 | 9.8 | 15.5 | 7.0 | 0.34 |
| 20 | Seattle | 0.7 | 337 | 2 | | 201 | 35.6 | 18.0 | 92.2 | 2.4 | 9.5 | 5.0 | 0.33 |
| 21 | Seattle | 0.7 | 337 | 2 | | 201 | 33.4 | 13.0 | 75.0 | 6.5 | | | |
| 22 | Seattle X-line N75E | 0.7 | 337 | 2 | | 201 | 33.2 | 17.7 | 68.9 | 0.9 | | | |
| 23 | Seattle X-line S85E | 0.7 | 337 | 2 | | 201 | 30.2 | 13.5 | 71.4 | 3.9 | | | |
| 24 | Quebec | 0.6 | 339 | 2 | 1.98 | 201 | 29.7 | 13.0 | 57.3 | 6.2 | 12.1 | 3.3 | 0.34 |
| 25 | Pittsburg 6 m | 0.5 | 340 | 4 | | 201 | 45.6 | 28.8 | 128.6 | 6.6 | 14.8 | 7.8 | 0.37 |
| 26 | Pittsburg 8 m | 0.5 | 340 | 4 | | 201 | 39.3 | 28.3 | 128.7 | 6.1 | | | |
| 27 | Pittsburg 2 m | 0.5 | 340 | 4 | | 89 | 61.8 | 21.8 | 122.2 | 1.1 | | | |
| 28 | Pittsburg 4 m | 0.5 | 340 | 4 | | 201 | 45.9 | 27.3 | 112.9 | 5.1 | | | |
| 29 | Sediment City | 0.5 | 75 | 3 | 2.57 | no data | | | | | 8.7 | 5.1 | 0.34 |
| 30 | Delaware | 1.5 | 133 | 3 | | 201 | 29.5 | 17.8 | 77.4 | 9.1 | 8.7 | 4.9 | 0.34 |
| 31 | 1 SE | 5.6 | 120 | 3 | 2.59 | 201 | 40.6 | 22.2 | 97.4 | 1.0 | 14.3 | 6.7 | 0.32 |
| 32 | 1 TSE | 6.0 | 135 | 4 | 2.15 | 201 | 48.9 | 19.7 | 92.1 | 6.9 | 16.1 | 8.9 | 0.33 |
| 33 | 2 SE | 3.4 | 104 | 0 | 1.56 | 201 | 31.3 | 9.2 | 53.5 | 9.9 | 10.8 | 3.7 | 0.30 |
| 34 | Baltimore site | 4.4 | 158 | 0 | 1.48 | 201 | 44.9 | 20.2 | 89.1 | 0.9 | 20.1 | 9.8 | 0.40 |
| 35 | Baltimore site | 4.4 | 158 | 0 | | 105 | 42.8 | 24.3 | 83.3 | 3.0 | | | |
| 36 | Baltimore ice line | 4.4 | 158 | 0 | | 201 | 47.0 | 18.8 | 92.9 | 14.5 | | | |
| 37 | Baltimore snow line | 4.4 | 158 | 0 | | 224 | 37.1 | 21.8 | 118.8 | 0.7 | | | |
| 38 | Baltimore smooth floe | 4.4 | 158 | 2 | | 1320 | 21.3 | 7.8 | 52.5 | 6.5 | | | |
| 39 | 1 north | 15.2 | 358 | 1 | 1.77 | 201 | 15.0 | 5.1 | 29.3 | 5.6 | 3.7 | 2.2 | 0.28 |
| 40 | 14 km north | 13.8 | 359 | 2 | | 151 | 23.6 | 9.1 | 40.7 | 5.3 | | | |
| 41 | 12 km north | 12.3 | 359 | 1 | | 151 | 11.1 | 2.5 | 17.3 | 6.3 | | | |
| 42 | 2 north | 11.1 | 359 | 1 | 1.43 | 201 | 14.1 | 4.5 | 26.9 | 6.5 | 4.0 | 1.7 | 0.28 |
| 43 | 10 km north | 10.3 | 6 | 2 | | 151 | 15.9 | 6.4 | 31.2 | 6.7 | | | |
| 44 | 8.6 km north | 8.6 | 2 | 3 | 1.98 | no data | | | | | | | |
| 45 | 3 north | 7.8 | 0 | 1 | 1.45 | 201 | 21.1 | 14.9 | 83.8 | 4.5 | | | |
| 46 | 4 north | 5.6 | 0 | 0 | | 201 | 37.8 | 23.9 | 114.5 | 1.6 | | | |
| 47 | 1 NW | 16.4 | 314 | 4 | 1.37 | 201 | 30.7 | 15.8 | 80.0 | 3.0 | 10.0 | 4.3 | 0.30 |
| 48 | 2 NW (14.7 km) | 14.7 | 315 | 4 | | 627 | 48.4 | 25.6 | 128.6 | 3.8 | | | |
| 49 | 3 NW (12.1 km) | 12.1 | 314 | 4 | | 601 | 29.7 | 16.9 | 91.2 | 4.7 | | | |
| 50 | 4 NW (9.5 km) | 9.5 | 314 | 4 | 1.71 | 201 | 33.5 | 20.6 | 96.3 | 5.1 | 8.7 | 8.2 | 0.27 |

**Table 1.** (continued)

| Number | Station | Distance, km | Bearing, degrees | Ice Code | Ice Thickness, m | *n* | Depth, cm | SD, cm | Maximum, cm | Minimum, cm | SWE, cm | SD, cm | Bulk Density, g/cm3 |
|---|---|---|---|---|---|---|---|---|---|---|---|---|---|
| 51 | 2 TSE | 7.2 | 136 | 2 | 1.81 | 201 | 18.2 | 7.0 | 35.8 | 4.1 | 4.6 | 3.6 | 0.26 |
| 52 | 3 TSE | 3.3 | 142 | 3 | 1.58 | 201 | 44.8 | 14.0 | 76.6 | 13.9 | 14.5 | 5.5 | 0.34 |
| 53 | 3 TSE | 3.3 | 142 | 3 | | 571 | 36.3 | 12.9 | 96.1 | 8.3 | | | |
| 54 | 3 TSE | 3.3 | 142 | 3 | | 616 | 34.5 | 14.3 | 109.9 | 1.0 | | | |
| 55 | 4 TSE | 4.8 | 139 | 1 | 1.74 | 201 | 21.6 | 8.5 | 41.9 | 8.6 | 6.2 | 3.6 | 0.29 |
| 56 | 5 TSE-N | 3.3 | 128 | 0 | 1.42 | 912 | 34.6 | 13.4 | 112.2 | 7.0 | | | |
| 57 | 5 TSE-E | 3.3 | 128 | 0 | | 645 | 36.1 | 12.9 | 90.2 | 1.4 | | | |
| 58 | 6 TSE-1 | 0.8 | 115 | 2 | 1.57 | 255 | 41.5 | 13.2 | 78.5 | 11.9 | | | |
| 59 | 6 TSE-2 | 0.8 | 115 | 2 | | 201 | 36.8 | 13.2 | 64.3 | 1.1 | | | |
| 60 | 6 TSE-3 | 0.8 | 115 | 2 | | 201 | 38.2 | 10.4 | 65.3 | 10.4 | | | |
| 61 | 6 TSE (with EM-31) | 0.8 | 115 | 0 | | 489 | 38.6 | 12.0 | 77.3 | 11.7 | | | |
| 62 | 1 west | 1.4 | 250 | 2 | | no data | | | | | 7.5 | 4.4 | 0.28 |
| 63 | Old Ridge1 | 3.3 | 106 | 4 | | 201 | 49.1 | 39.1 | 128.4 | 7.3 | | | |
| 64 | Old Ridge 2 | 3.3 | 106 | 4 | | 155 | 41.9 | 32.1 | 128.5 | 1.5 | | | |
| 65 | Wilmington | 4.3 | 126 | 3 | 1.78 | 153 | 18.1 | 6.9 | 43.5 | 1.1 | 5.5 | 3.1 | 0.29 |
| 66 | peak radar | 2.5 | 119 | 3 | | 510 | 32.5 | 10.1 | 61.2 | 1.4 | | | |
| 67 | main snow line 0–187 | 0.5 | 340 | 0 | | 187 | 42.1 | 23.1 | 111.6 | 6.4 | | | |
| 68 | main snow line 0–374 | 0.5 | 340 | 0 | | 375 | 30.5 | 16.0 | 108.4 | 0.9 | | | |
| 69 | main snow line | 0.5 | 340 | 0 | | 632 | 29.6 | 19.5 | 110.6 | 1.0 | | | |
| 70 | ridge at Delaware | 2.0 | 105 | 0 | 1.31 | 246 | 44.7 | 13.4 | 83.8 | 0.9 | 17.3 | 4.1 | 0.36 |

[a]Ice codes: 0 = not classified; 1 = leads, 2 = refrozen melt ponds; 3 = hummocky ice; 4 = ridges and rubble fields.

undeformed ice the late winter increase was minimal. This late winter differentiation in depth resulted from wind transport of snow leading to drift accumulation near ridges and scouring in more neutral locations, a fact reflected in the continually increasing standard deviation of depth (SD in Figure 2b) during the winter at the main snow line, which included both ridges and undeformed ice.

[9] The buildup of the snow cover was the result of the deposition and subsequent metamorphism of the 10 layers of snow shown in Figure 3 and described in Table 2. Similar stratigraphy was observed in almost all snow pits ($n$ = 195), though wide variations in layer thickness, density, hardness, and degree of metamorphism were common. At any given site, one or more layers might be missing, in which case the snowpack was thinner. As will be shown later, missing layers were more likely to be observed in areas of smooth ice, and typically, the missing layers were from higher in the stratigraphic column.

[10] Layers were composed of one of three basic types of snow: depth hoar (layers *b*, *c*, *d*, and *e*), wind slab (layers *f*, *g*, and *j*), or recent (layers *h* and *i*)(Figure 3). In addition, at the base of the pack there was a thin, intermittent layer of snow ice (layer *a*). The depth hoar, a low-density, brittle, highly permeable type of snow with low thermal conductivity and large ornate grains (5–15 mm) [*Trabant and Benson*, 1972; *Akitaya*, 1974] formed both at the base of the snow and near the surface of the SHEBA snowpack. Strong gradients in early winter turned layers *b* through *d* into "classic" depth hoar, while diurnal temperature cycling in April and May resulted in near-surface kinetic growth [*Birkeland*, 1998] that produced small (0.5 mm) but distinctively faceted depth hoar-like crystals in near-surface layers. Wind slab, a fine-grained (0.3 to 0.8 mm), dense, well-bonded type of snow with high thermal conductivity, formed during storms when snow grains were tumbled by the wind, breaking them and producing smaller grains which packed together and sintered into a strong, well-bonded layers [*Seligman*, 1980; *von Eugster*, 1950]. The most conspicuous example at SHEBA was layer *f*, which formed when some of the highest and most sustained winds of the winter occurred. The recent snow had a wide range of grain characteristics that depended on meteorological conditions during snowfall [*Nakaya*, 1954; *Magono and Lee*, 1966], but generally was of low-density and low thermal conductivity. After deposition, it metamorphosed and compacted rapidly in response to gravitational settlement and fluctuations in temperature.

[11] The snow layers comprising the SHEBA snow cover (Figure 3) were produced by 10 fairly discreet weather events (defined as continuous periods of precipitation, wind, or wind plus precipitation), as shown in Figure 4. Most of the events were short-lived, less than 24 hours in length. However, the events responsible for the formation of the two most prominent snow layers in the pack (wind slabs *f* and *g*) were multiday storms with combined wind and snow. Even including these, however, the combined time for all the key weather events constituted only a small fraction of the entire winter (~6%). Unfortunately, the first layer-producing events of the 1997–1998 winter occurred before we arrived at the SHEBA site and were not witnessed. They had deposited about 10 cm snow, of which the bottom layers had been converted into snow ice.

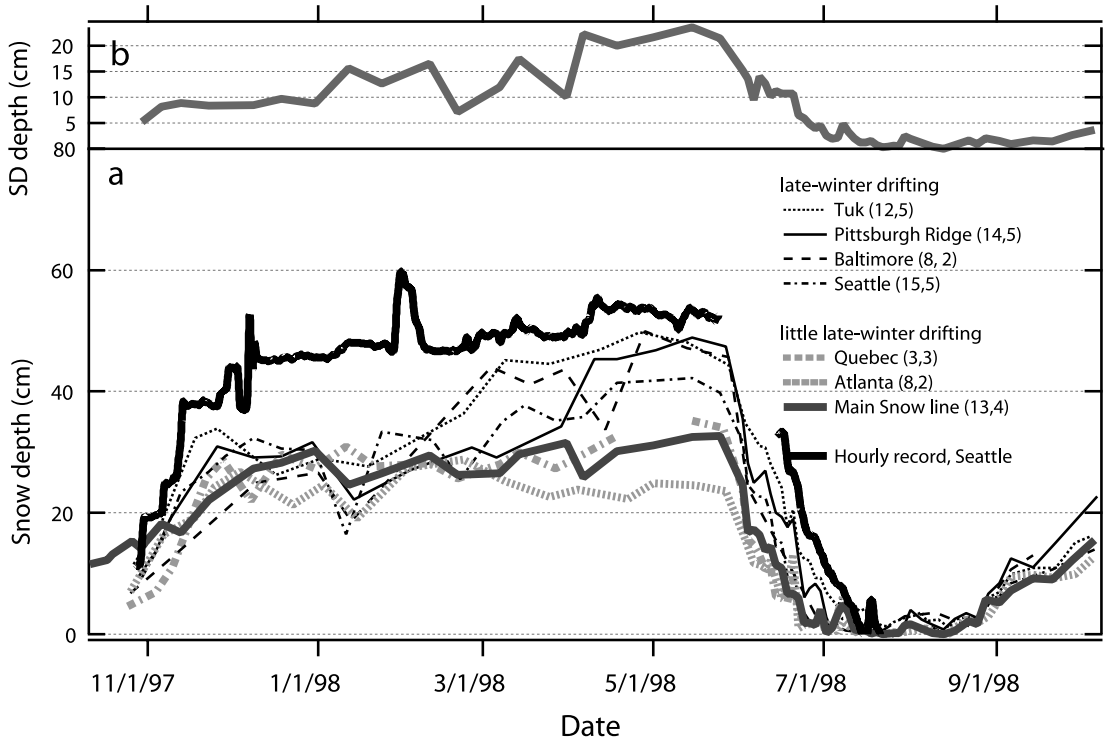


**Figure 2.** The increase in snow depth through the winter of 1997–1998, SHEBA camp. The heavy black line is an hourly record from a sonic sounder at Seattle. It came into operation on 1 November 1997. The heavy gray line is the depth from the stakes on the main snow line, for which observations start on 11 October, at which time there was 11 cm of snow. Other lines are average values from stake lines in the vicinity of SHEBA. The numbers in parentheses after the line names indicate the number of stakes used in computing the values, and the number of stakes excluded due to depths affected by drifting or scouring. The record from Seattle increases more rapidly than the others because snow drifted into the small refrozen melt pond where the sonic sounder was located. The SD of depth for the main snow line is shown at the top.

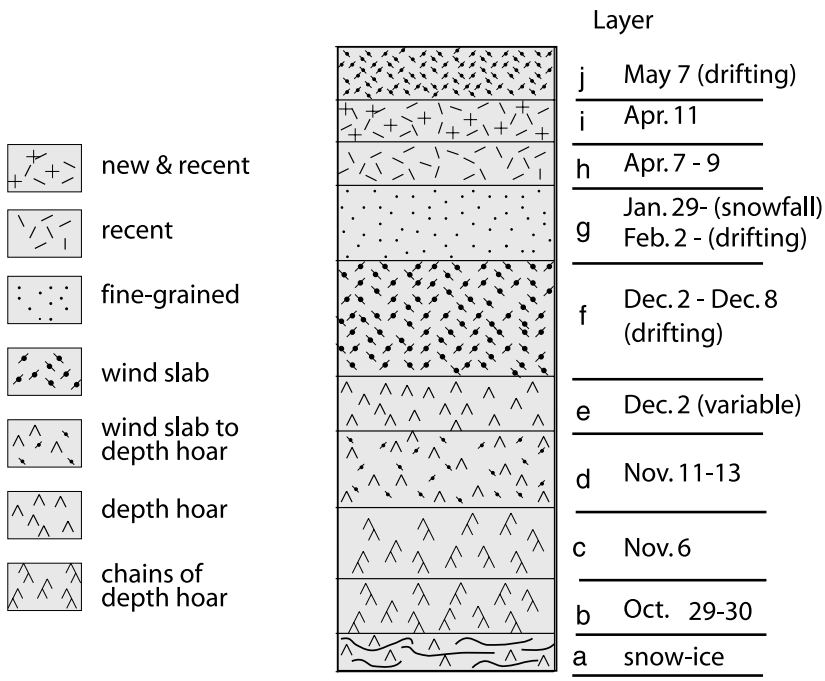


**Figure 3.** Generalized snow stratigraphy column for the SHEBA area, 1997–1998. Symbols follow the International Classification for Snow on the Ground [*Colbeck et al.*, 1992]. Dates indicate the approximate time when the layer was deposited. The snow ice was derived from snow that had fallen before we arrived at the site. Layers *h* and *i* were so similar they could rarely be differentiated in the field.

**Table 2.** Snow Layer Characteristics at SHEBA, 1997–1998

| Unit | Parameter | Snow Code | Density, g/cm3 | Hardness | Thickness, cm | SWE, cm | Percent Total SWE | kbulk, W/m K |
|---|---|---|---|---|---|---|---|---|
| *j* | average | 6 | 0.316 | 3 | 4.8 | 1.5 | 9 | 0.203 |
| *n* = 11 | SD | | 0.064 | 1 | 3.3 | | | 0.000 |
| *i* | average | 2 | 0.187 | 1 | 4.2 | 0.8 | 5 | 0.087 |
| *n* = 199 | SD | | 0.068 | 1 | 2.8 | | | 0.060 |
| *g* | average | 5 | 0.321 | 2 | 6.9 | 2.2 | 13 | 0.164 |
| *n* = 103 | SD | | 0.061 | 1 | 6.0 | | | 0.068 |
| *f* | average | 7 | 0.403 | 4 | 10.7 | 4.3 | 26 | 0.264 |
| *n* = 201 | SD | | 0.061 | 1 | 9.3 | | | 0.070 |
| *d* | average | 9 | 0.344 | 3 | 7.5 | 2.6 | 16 | 0.182 |
| *n* = 85 | SD | | 0.072 | 1 | 6.0 | | | 0.070 |
| *c* | average | 12 | 0.279 | 2 | 6.5 | 1.8 | 11 | 0.087 |
| *n* = 182 | SD | | 0.056 | 1 | 5.1 | | | 0.033 |
| *b* | average | 13 | 0.343 | 3 | 5.1 | 1.8 | 11 | 0.270 |
| *n* = 102 | SD | | 0.132 | 1 | 4.7 | | | 0.236 |
| *a* | average | 15 | 0.507 | 5 | 3.1 | 1.5 | 9 | 0.528 |
| *n* = 9 | SD | | | | | | | |

| Hardness | Code | Snow Type | Code | Snow Type | Code |
|---|---|---|---|---|---|
| Fist | 1 | new | 1 | very hard slab | 8 |
| Four fingers | 2 | recent | 2 | slab to hoar | 9 |
| One finger | 3 | fine-grained | 3 | depth hoar | 10 |
| Pencil | 4 | medium-grained | 4 | chains of hoar | 11 |
| Knife | 5 | soft slab | 5 | chains of hoar, indurated | 12 |
| Ice | 6 | moderate slab | 6 | chains of hoar, voids | 13 |
| | | hard slab | 7 | icy hoar | 14 |
| | | | | snow ice | 15 |

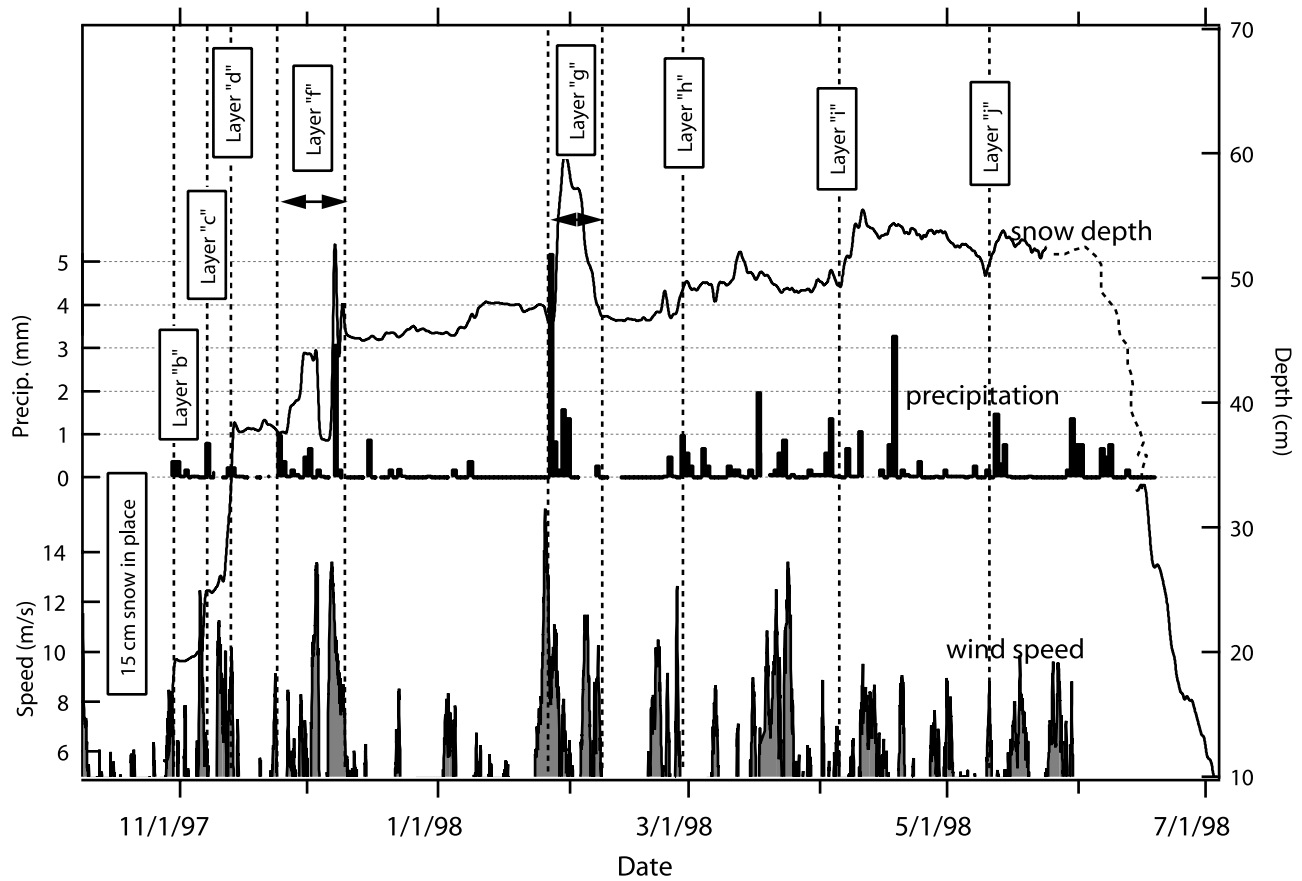


**Figure 4.** Snow layer formation as determined from correlation of weather records with the snow depth at the Seattle station. See Figure 3 for layer descriptions. As discussed in the text, the timing of the precipitation from the Nipher-shielded gauge is thought to be reliable, but the amount is not.

[12] Many events in the weather record that might have been expected to produce a stratigraphic layer did not (Figure 4). In total, the record contained about 30 precipitation events and at least 26 periods when winds were sufficiently fast to transport snow (usually assumed to be between 4 and 6 m $s^{-1}$ [*Kuz'min*, 1963; *Takeuchi*, 1980]). This was particularly true during the middle and end of the winter (February to April) when numerous small snowfall events produced only a few, relatively thin layers of snow (layers *h*, *i* and *j*). These layers were more discontinuous than layers lower in the pack and contained an insignificant amount of snow water equivalent (SWE) (Table 2). One reason for the dearth of late winter layers is that during the middle and end of winter, simultaneous wind and snowfall was not common, except during the event that formed slab *g*. Another reason may be that precipitation amounts were lower during this period than earlier in the winter (Figure 4, middle), as discussed below.

[13] Winter precipitation is notoriously hard to measure in a windy environment. The precipitation values shown in Figure 4 come from a Nipher-shielded gauge (R. Moritz, personal communication, 2000; see www.joss.ucar.edu/cgi-bin/codiac/fgr_form/id=13.735) and have been corrected following the method of *Goodison and Yang* [1996]. In a windless environment, the gauge performs well [*Goodison et al.*, 1981], but in windy conditions it undercatches the true snowfall by a substantial amount, a problem that has been widely investigated [*Black*, 1954; *Benson*, 1982]. The average correction factor applied to the SHEBA winter precipitation data was 2.5. Despite this correction, the total cumulative winter precipitation was less than the snow water equivalent observed on the ice. For example, during the first three snowfalls of the season (those that produced layers *b*, *c*, and *d*), the recorded precipitation at the Nipher-shielded gauge totaled 0.9 cm. Based on the area-wide average thickness and density of these three layers (Table 2), at least 5 cm of precipitation must have fallen. For the entire winter, the mean snow depth at SHEBA was 33.7 cm and the mean density was 0.34 g $cm^{-3}$ (see section 3.2), giving a mean on-ice SWE of 11.6 cm. The cumulative total based on the corrected gauge record for the same period was 8.6 cm, or approximately 74% of the SWE on the ice. Sublimation losses from the snowpack (which would not have affected the Nipher gauge) would drop this percentage another 5 to 20% [*Pomeroy and Gray*, 1995], suggesting that the recorded precipitation was between 1/2 and 2/3 of the actual winter total. Because of these difficulties, we place more reliance on the timing of the winter precipitation than on its absolute magnitude. We also suggest, based on the fact that no distinct stratigraphic layers were added in middle and late winter, that there was less precipitation later in the winter than earlier, despite the fact that in the gauge recorded a fairly even rate of precipitation throughout the winter.

[14] The weather records and snow stratigraphy suggest dividing the winter into five distinct stages:

1. Ephemeral: During this stage, most of which occurred before formal measurements began at SHEBA, snow fell on wet ice and was subjected to above freezing temperatures. These conditions changed some of the snow into a snow-ice layer (layer *a* in Figure 3), which in places must have melted away completely since it was observed only intermittently.

2. Rapid buildup: A quick sequence of storms in late October and early November led to a rapid buildup of the pack. Over 30 cm of snow (Figures 2 and 3; layers *b*, *c*, and *d*) was deposited in the space of about two weeks. In some cases (layer *d*), the snowfall was accompanied by wind sufficient to cause drifting and noticeably higher densities ($\rho$ = 0. 343 g $cm^{-3}$). In other cases (layer *c*), high wind preceded the precipitation but was dropping as it began to snow, producing a low-density layer. Because all three layers (*b*, *c*, and *d*) arrived early in the winter, they were subjected to strong temperature gradients for periods longer than any other layers. By April, when they were examined in detail, all three had metamorphosed into an extreme form of depth hoar with conspicuously large grains and very low values of thermal conductivity [see *Sturm*, 1991].

3. Winter storms: From late November to May, the only significant changes in the snowpack occurred when two prolonged storms added wind slab layers to the pack. Layer *f* was created during a weeklong sequence of snow and high winds (>12 m $s^{-1}$) that started on 1 December 1997 (Figure 5). By the end of the storm, a thick, dense, hard wind slab capped the underlying layers everywhere. The upper surface of this layer was sculpted into dunes, barchans, and sastrugi that played an important role in the deposition of subsequent snow layers. Layer *g* was deposited during a less vigorous storm between 29 January and 7 February. Unlike the deposition of layer *f*, in which the high wind coincided with snowfall, layer *g* was deposited as the wind speed was dropping. It was half the thickness of layer *f* and not nearly as hard. Layer *f* could only be penetrated by a knife, or occasionally by a pencil, while *g* could be penetrated by a pencil, or more often, a finger. Combined, layers *f* and *g* accounted for 39% of the total pack SWE (Table 2).

4. Spring flurries: A series of small, inconsequential snowfall events began in mid-March and lasted until the snowmelt started on 29 May. These events deposited many thin, soft snow layers, which were either immediately or subsequently reworked by the wind producing layers that were itermittent and often difficult to discriminate (i.e., *h* from *i*). This series of small snowfalls led to a limited increase in the snow depth, adding less than 15% to the total SWE.

5. Melt: Continuous snowmelt began on 29 May 1998.

[15] The critical dependence of snow properties on the combined timing of wind and snowfall can illustrated using the development of layer *f* (Figure 5). During a three-day period in late November, light snow with wind resulted in the accumulation of about 7 cm of snow. On 3 December the wind rose to 14 m $s^{-1}$ and began to erode and transport this new snow, starting the development of a slab. However, it was not until 8 and 9 December, when there was simultaneous heavy snowfall and high wind, that the most of the slab was deposited and its characteristics fixed. Equally high winds were observed at other times during the winter, in some cases following recent snowfalls, but they failed to produce thick, dense slabs. For the deposition of layer *f*, the combination of snow and wind was critical.

[16] One reason why simultaneous snow and wind might have been necessary for the development of a major slab layer like *f* is that the air layer immediately above the snow surface was frequently supersaturated with water vapor [*Andreas et al.*, 2002]. The moisture came from abundant leads in the vicinity of the field area and is a common

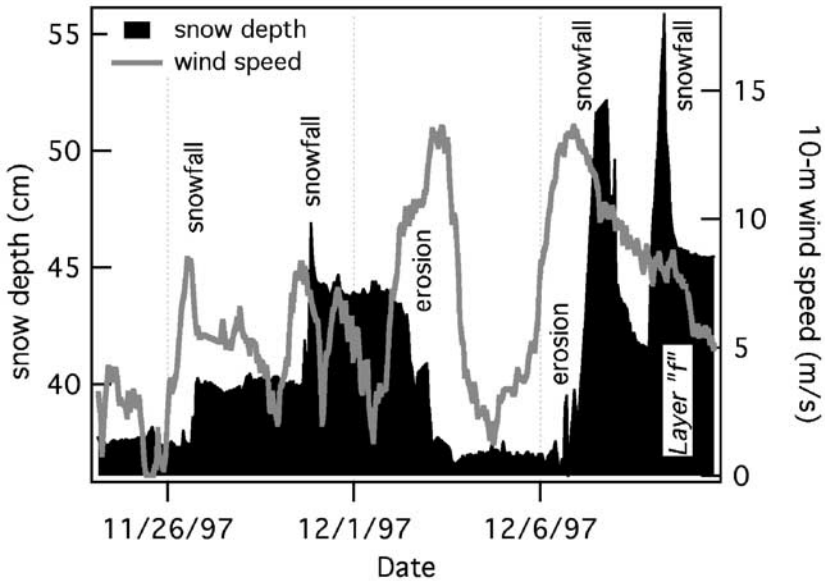


**Figure 5.** The formation of the *f* slab in December 1997.

occurrence over sea ice. *Radionov et al.* [1997] measured condensation rates at the snow surface as high as 1 mm month$^{-1}$. The condensation occurs at the snow surface because it is often colder than the air above it [*Nyberg*, 1938]. If this process was occurring at SHEBA, it must have been subtle: We could not detect riming or hoar frost formation and the snow often looked pristine and new. However, recent snow that appeared to be unaltered was observed to resist transport at wind speeds that should have been sufficient to move the snow. We surmise that surface riming and hoarfrost formation may have increased the critical surface shear stress and therefore the wind speed necessary for transport. Between 1 April and 15 May, at least 10 wind events in excess of 6 m s$^{-1}$ occurred, and yet during this time, little or no transport of snow layers was observed.

[17] Unlike the episodic formation of wind slabs, depth hoar formation was continuous throughout the winter. Winter air temperatures were consistently low, while ice surface temperatures were relatively high, so the temperature gradient across the snowpack was often extreme and kinetic crystal growth proceeded to a remarkable degree. Layers *b*, *c*, *d*, and *e* were subjected to mean temperature gradients that were about 1.5 times greater than those considered necessary for the development of depth hoar (Figure 6) [see *Marbouty*, 1980; *Armstrong*, 1985]. Layers higher in the pack (*f*, *g*, *h*, and *i*) were subjected to depth hoar forming gradients intermittently. It is not surprising, then, that by late winter the entire lower half of the snowpack had turned into depth hoar. Even layers that had been worked by the wind, such as layer *f*, in places had been converted by the extreme temperature gradients. The development of depth hoar in the lower part of the pack was also aided by the presence of a substrate (ice) that could serve as a source of moisture for depth hoar growth, a phenomenon that has been discussed by *Sturm and Benson* [1997].

[18] Using depth hoar crystal growth rates [*Fukuzawa and Akitaya*, 1993], measured temperature gradients (Figure 6, open triangles), and the length of time these gradients prevailed in each layer of snow, we have computed the size of the depth hoar crystals in each layer of snow (Figure 6, bottom axis). The estimates indicate grains in the lowest four layers of snow would have been 10 mm or larger. Higher in the pack, the grain size would have fallen off rapidly (Figure 6). These estimates are encouragingly close to observed sizes; basal layers *b*, c, and *d* had crystals in excess of 10 mm, while the upper layers had crystals that were only 2–4 mm in size.

[19] While time series measurements of snow layer density were not made at SHEBA, we can infer, based on analogy with snow of similar characteristics elsewhere

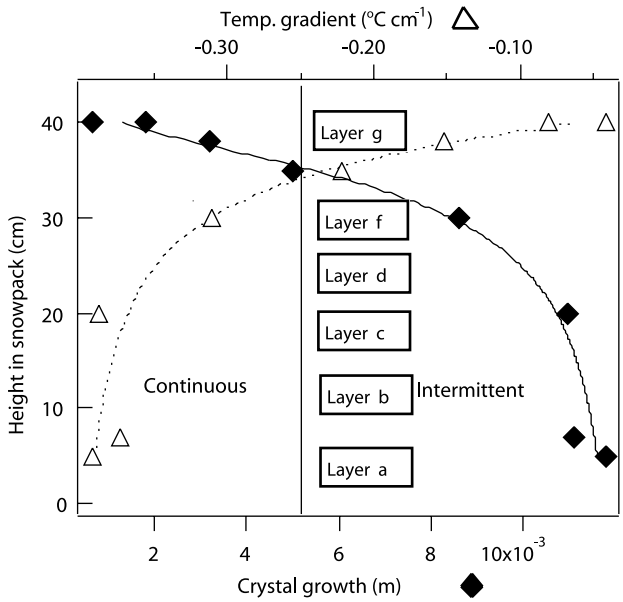


**Figure 6.** Average temperature gradients (top axis) and depth hoar crystal growth (bottom axis) keyed to stratigraphic layers. The critical gradient necessary for the formation of depth hoar (−0.25°C cm$^{-1}$) [*Marbouty*, 1980; *Armstrong*, 1985] is shown as a vertical line.

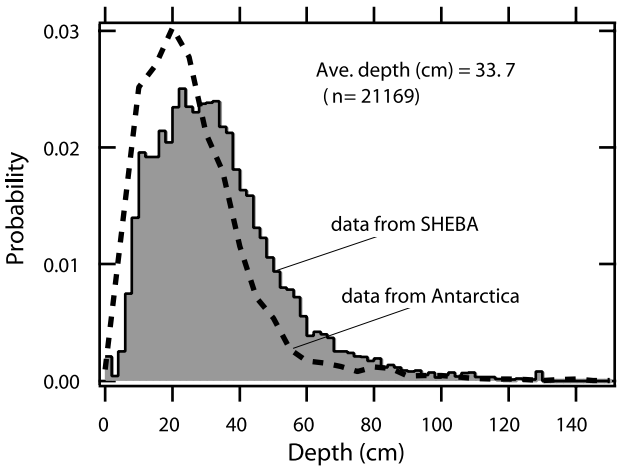


**Figure 7.** The probability distribution function (PDF) for all SHEBA snow depths, compared with a PDF for snow on ice in the Bellinghausen, Ross, and Admundsen Seas, Antarctic [*Sturm et al.*, 1998].

[*Sturm and Holmgren*, 1998] that the densities measured at the end of the winter (Table 2) were not much different than earlier in the winter. *Armstrong* [1980] and *Sturm and Benson* [1997] have shown that depth hoar is "stiff" in vertical compression, undergoing only limited compaction. It is also often subjected to an upward vapor flux. Combined, these result in a density that is nearly constant [*Trabant and Benson*, 1972; *Sturm*, 1991; *Sturm and Benson*, 1997]. Similarly, wind slab layers tend to be deposited at such high density that once deposited, they do not compact much [*Sturm and Holmgren*, 1998]. Moreover, the total overburden pressure of the thin SHEBA snowpack was too low to affect much compaction on any type of snow.

### 3.2. Regional-Scale Variability of Depth, Density, and Stratigraphy ($\sim 10^4$ m)

[20] During April and May, snow depth was measured at 21,169 places near the SHEBA site. The mean depth was 33.7 cm with a standard deviation of 19.3 cm and a median of 30.5 cm. Depths ranged from 0 to 150 cm (Figure 7). About 5.8% of the area, primarily thin ice and the tops of ridges, was covered by less than 10 cm of snow, while about 3.9% of the area, pockets adjacent to ridges, were filled by deep drifts (>80 cm). A comparison of the probability distribution function (PDF) for the SHEBA snow depths with a PDF of winter snow depths from the Amundsen, Bellinghausen, and Ross seas in Antarctica [*Sturm et al.*, 1998] (Figure 7) suggests that there was a higher percentage of deep snow areas in the Arctic than the Antarctic. This difference is probably the result of a higher concentration of ridges, and taller ridges, in the Arctic.

[21] Based on field sampling, snowdrifts associated with ridges occupied between 3 and 6% of the total SHEBA study area, depending on the method of calculation. The drifts typically extended 15 to 25 m from the ridge crests in both directions, but not all of this area had enhanced snow depths. In fact, at ridge crests and out near the tails of the drifts the snow was often shallower than the snow on level floes. In some places it was even scoured away. For the 14 stations (Table 1) that included distinctive ridge snowdrifts, we have computed that the drift sections had mean depths that on average were 30% higher than the surrounding snow. Had there been no ridges and therefore no drifts, the mean depth at SHEBA would have been about 33 cm, a decrease of less than a centimeter from the value determined using all the measured depths. Of course, there would have been no really deep snow then, and the right-hand tail of the PDF in Figure 7 would have been truncated.

[22] The SHEBA PDF for depth can be converted into one for snow water equivalent (SWE) using the results in Figure 8, which indicate that there was a strong linear relationship between depth and SWE. For all data ($n = 362$):

$$\mathrm{SWE(cm)} = 0.348*\mathrm{depth(cm)} \quad (1)$$

with an $r^2$ of 0.975 and a standard error of 0.003. A slight improvement is achieved if the regression in equation (1) is limited to depths less than 80 cm, thereby excluding drifts:

$$\mathrm{SWE(cm)} = 0.343*\mathrm{depth(cm)} \quad (2)$$

with $n$ now equal to 357 and an $r^2$ of 0.987.

[23] The value 0.343 is effectively the bulk density of the SHEBA snow cover. The high $r^2$ arises for two reasons: (1) SWE is the product of depth times density, and (2) the bulk density of the snow (the slope of the line in Figure 8) was basically independent of the snow depth and did not vary with ice type. This independence of ice type can be seen in the plot of residual values shown at the top of Figure 8, where no pattern is apparent. Given the contrasts in density between layers *f* and *c*, for example, and the large standard deviations (SD) in layer thickness (Table 2), the finding is somewhat surprising. There was also no significant change in the bulk density during the six-week period that the measurements were made. During that time, layers *h*, *i*, and *j* were added to the snowpack, but as stated before, these layers contributed little to the total SWE. This spatial and temporal invariance in the bulk density is convenient because it allows depth to be converted to SWE with reasonable accuracy over the entire SHEBA area, and over a relatively long period during the winter.

[24] While bulk density was relatively invariant with ice type, snow depth was not. The SHEBA PDF for all depths shown in Figure 7 can actually be thought of as a composite of distinct PDFs from several different types of ice. To identify these individual PDFs, we divided the 70 stations at which depths and other snow properties were measured into four ice classes (Table 1). These classes were determined from the field observations we could make most readily, namely the ice topography, the surface roughness, and the ice appearance revealed in the bottom of snow pits. In increasing order of roughness and snow-holding capacity, the classes were: (1) smooth ice (mostly refrozen leads and undeformed first-year ice), (2) multiyear ice containing large refrozen melt ponds and slightly rougher first year floes, (3) hummocky multiyear ice floes with and without small melt ponds, and (4) deformed ice (rubble fields and ridges). The classes actually form a continuum, but in general there was a strong consensus between observers as to which class a particular measurement station should be assigned. In some cases, the 100 m long lines on which snow depth and other snow properties were measured passed

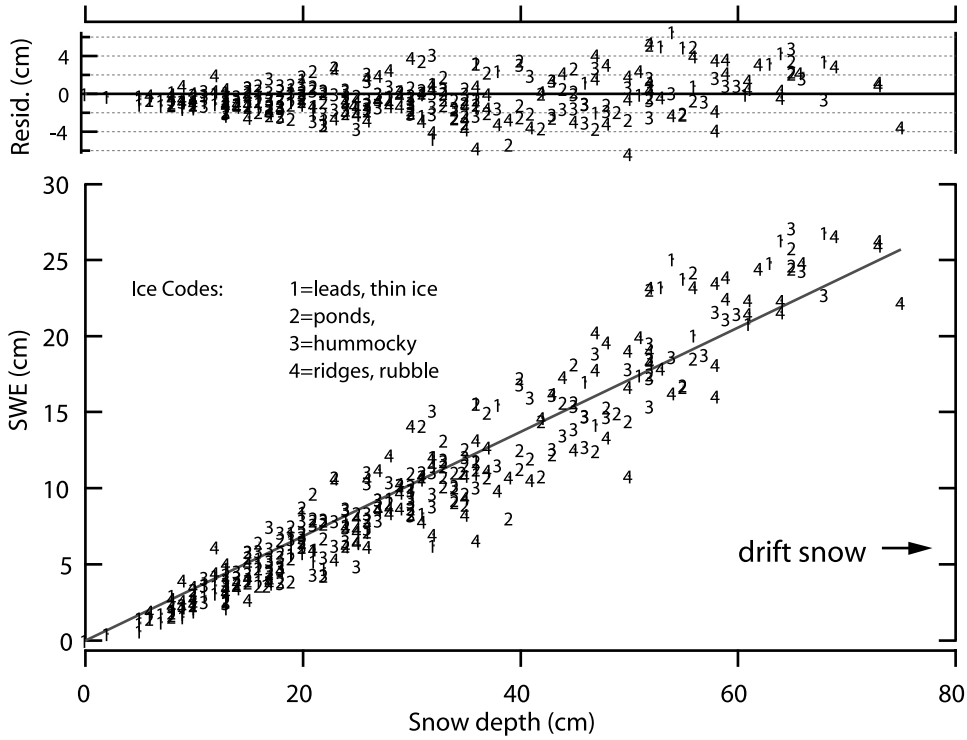


**Figure 8.** Snow water equivalent (SWE) versus depth with residuals and symbols by ice type. We have excluded sample points for depths in excess of 80 cm because they are from drifts, which typically are denser than the general snowpack.

from one class of ice to another; in these cases, only the subsections of the line in a single class of ice have been used in our analysis. In Figure 9 the snow depth PDF from the "purest" example of each class of ice is shown. These PDFs illustrate that as the snow holding capacity and ice roughness increased, the mean depth and the standard deviation (SD) (as evidenced by the spread of the PDF) also increased. When combined (and weighted by the areal fractions of the various ice classes), the individual PDFs form a PDF that is similar to the one shown in Figure 7 (Actually, it is a little messy since the four PDFs shown in Figure 10 comprise only 804 points versus the 21,169 in Figure 7). Plotting the SD as a function of mean depth, distinct but overlapping fields of ice type were observed (Figure 10).

[25] To test the significance of the observed variation in depth and SD by ice class, we used an ANOVA [*Davis*, 1986] with a Tukey HSD pairwise mean comparison test [*SYSTAT*, 1989]. These tests show that at the 90% confidence level, the snow depth differed across all four classes of ice with the exception that no significant difference existed between classes 2 and 3 (refrozen ponds and hummocky ice floes). This result could have been anticipated: it was often difficult to differentiate classes 2 from 3 in the field. For the SD of depth, the differentiation by class was not as distinct; only the deformed ice class (ridges and rubble fields) could be differentiated from the other three. The same was true for the SWE; only the SWE from deformed ice class differed significantly from the other classes (90% confidence interval).

[26] Variation in snow stratigraphy by ice class was even more complicated (Table 3). As expected, the number of layers and their thickness tended to increase with increasing snow depth. Because of the positive relationship between snow depth and ice type, the number of layers and layer thickness therefore increased as the ice class went from 1 to 4. In other words, there were more snow layers in rubble fields and near ice ridges than on smooth ice, and the layers were thicker. The number of layers tended to increase with ice class more rapidly than the thickness of the layers, a observation consistent with the fact that near ridges and in rubble fields snow layers were rarely scoured away and therefore less likely to be missing than on smoother classes of ice. The type of snow, represented in a simple fashion by the depth hoar and wind slab fractions (Table 3), tended toward a equal mix where the snow was deeper and the ice was rougher (i.e., class 4). When the snowpack tended to be mostly wind slab and not much depth hoar (or the reverse), then it was likely to be found on the smoother classes of ice (1 and 2).

### 3.3. Local-Scale Variability of Depth, Density, and Stratigraphy ($\sim 10^2$ m)

[27] The PDFs in Figure 9 suggest that even on ice floes that were relatively homogenous and could be classified as a single type of ice, considerable local spatial variability in snow depth could be found. Mapping the depth verified this fact. Data collected from a flat portion of a multiyear floe (Figure 1, station "Sediment City," ice class 3) with no visible ridges or structural breaks showed a snow cover whose depth varied by a factor of six over distances as short as 20 m (Figure 11) and an irregular horizontal alternation of patches of thick and thin snow ranging from 15 to 40 m in length. A cross section (Figure 11, top left) through the map area showed that the variation in depth arose from a combination of undulations in the ice surface and drifts at the snow surface. Two long probe lines (each

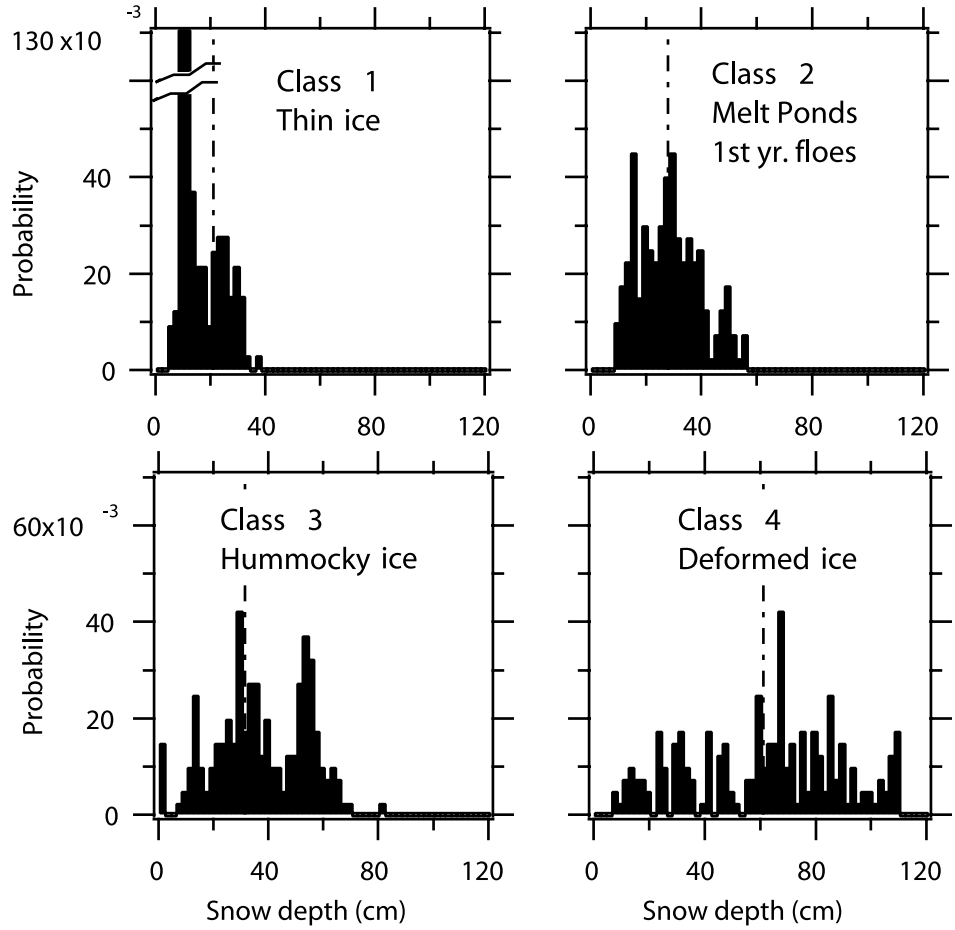


**Figure 9.** Probability distribution functions for the four classes of ice. The vertical dot-dash line indicates the mean depth at the station.

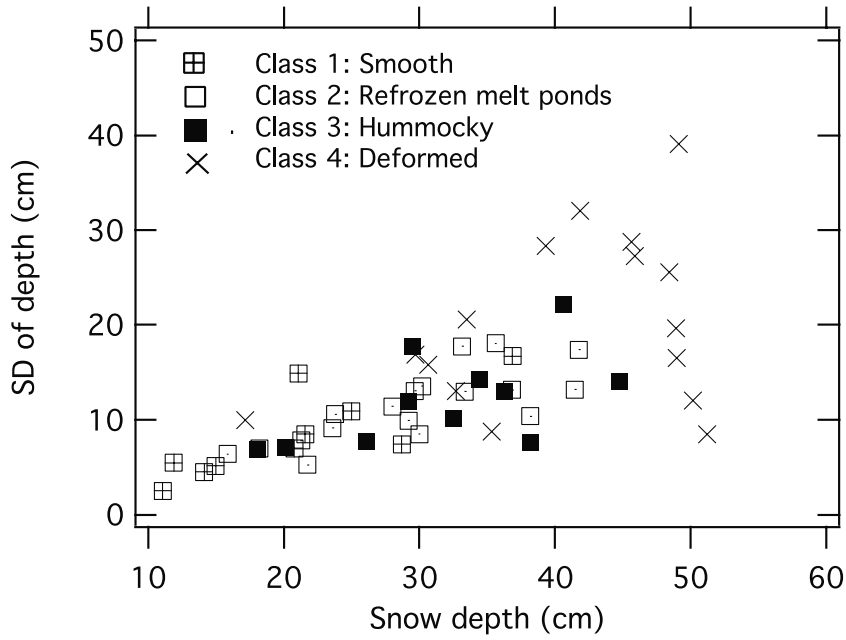


**Figure 10.** Standard deviation of depth (SD) as a function of average depth for all stations where an unambiguous classification of the ice could be made. In most cases, 201 measurements were taken at each station and have been used to compute the mean and SD. In cases where snow depth traverse lines extended across two or more ice classes, only portions of the station data have been used.

**Table 3.** Stratigraphic Characteristics for Each Station Where Snow Stratigraphy was Measured

| Station | Ice Code | Bulk Density, g/cm3 | Number of Layers | Average Layer Thickness, cm | Total Thickness, cm | Hoar Fraction | Slab Fraction |
|---|---|---|---|---|---|---|---|
| Atlanta | 2 | 0.355 | 3.6 | 8.8 | 31.0 | 0.303 | 0.643 |
| Atlanta triangle | 3 | 0.347 | 5.3 | 6.8 | 36.0 | 0.400 | 0.462 |
| 2 east | 2 | 0.326 | 5.5 | 7.7 | 39.7 | 0.247 | 0.453 |
| 1 east | 1 | 0.221 | 2.7 | 3.9 | 10.5 | 0.153 | 0.300 |
| Tuk | 4 | 0.345 | 4.3 | 5.3 | 26.3 | 0.450 | 0.383 |
| Tuk lead | 0 | 0.347 | 4.8 | 17.4 | 38.2 | 0.349 | 0.637 |
| Tukx | 4 | 0.302 | 5.0 | 4.0 | 20.5 | 0.287 | 0.445 |
| 3 NE | 3 | 0.287 | 4.9 | 4.5 | 21.3 | 0.134 | 0.474 |
| 1 NE | 2 | 0.359 | 3.5 | 4.8 | 15.7 | 0.172 | 0.567 |
| Seattle | 2 | 0.337 | 6.0 | 6.9 | 42.5 | 0.267 | 0.469 |
| Quebec | 2 | 0.328 | 4.5 | 6.6 | 30.5 | 0.307 | 0.496 |
| Pittsburg | 4 | 0.358 | 6.8 | 6.2 | 43.0 | 0.290 | 0.509 |
| Sediment City | 3 | 0.332 | 5.4 | 4.7 | 27.7 | 0.369 | 0.336 |
| Delaware | 3 | 0.339 | 4.5 | 7.1 | 27.8 | 0.196 | 0.489 |
| 1 SE | 3 | 0.295 | 7.7 | 6.3 | 48.8 | 0.388 | 0.309 |
| 1 TSE | 4 | 0.304 | 5.7 | 8.7 | 47.5 | 0.219 | 0.368 |
| 2 SE | 0 | 0.325 | 5.7 | 6.1 | 35.0 | 0.363 | 0.327 |
| Baltimore | 0 | 0.379 | 4.7 | 10.4 | 50.0 | 0.457 | 0.516 |
| 1 N | 1 | 0.314 | 2.7 | 4.7 | 13.2 | 0.141 | 0.463 |
| 2 N | 1 | 0.285 | 3.0 | 5.1 | 14.0 | 0.551 | 0.394 |
| 3 N | 1 | 0.258 | 3.2 | 4.1 | 13.4 | 0.540 | 0.265 |
| 4 N | 0 | 0.330 | 4.5 | 8.6 | 36.5 | 0.420 | 0.330 |
| 1 NW | 4 | 0.292 | 4.8 | 7.1 | 33.3 | 0.333 | 0.128 |
| 4 NW | 4 | 0.266 | 5.2 | 5.5 | 29.5 | 0.620 | 0.181 |
| 2 TSE | 2 | 0.307 | 3.8 | 4.7 | 17.5 | 0.575 | 0.269 |
| 3 TSE | 3 | 0.325 | 4.7 | 9.6 | 44.7 | 0.528 | 0.396 |
| 4 TSE | 1 | 0.312 | 3.8 | 5.8 | 22.5 | 0.371 | 0.523 |
| 5 TSE | 3 | 0.315 | 5.6 | 6.2 | 35.2 | 0.524 | 0.400 |
| 6 TSE | 2 | 0.331 | 4.6 | 8.9 | 39.7 | 0.611 | 0.365 |
| 1 West | 2 | 0.328 | 5.0 | 6.7 | 32.0 | 0.487 | 0.513 |
| Ridge | 4 | 0.350 | 7.0 | 19.3 | 135.0 | 0.367 | 0.474 |
| Wilmington | 3 | 0.306 | 3.2 | 5.1 | 14.6 | 0.255 | 0.517 |
| Peak | 3 | 0.338 | 4.7 | 8.7 | 37.6 | 0.435 | 0.491 |
| Averages | | 0.320 | 4.7 | 7.2 | 33.7 | 0.37 | 0.42 |

> 300 m) forming an "X" near the map area (Figure 1) confirmed that the variations were widespread.

[28] The 20 m patch size visible in Figure 11 was a consistent feature throughout the SHEBA area. From semivariograms [*Isaaks and Srivastava*, 1989] of the longer snow depth probe lines (Figure 12), we found that the dominant structural size fell in a narrow band centered on 20 m (it varied from about 13 to 30 m). A semivariogram describes the spatial variation in a property as a function of the distance between sampling points using two main descriptive variables, the range, and the sill [*Clark*, 1980]. The range is a good measure of structural length. In this case,

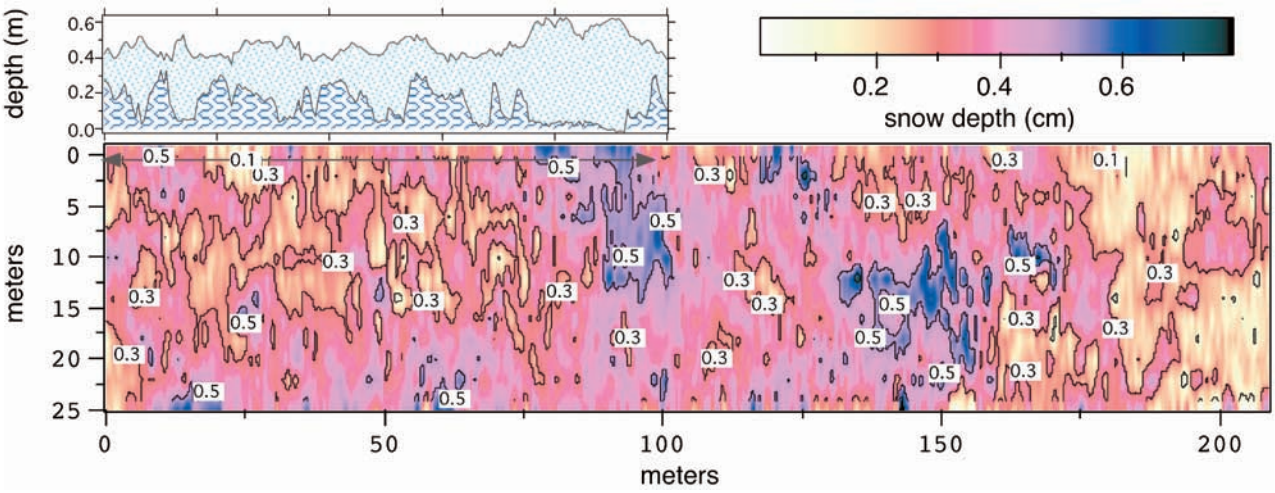


**Figure 11.** A snow depth map from station Sediment City (Figure 1) derived from 11,531 radar measurements. It suggests that homogeneous areas of depth were on the order of 20 m in length. The cross section (top left) was measured in the area shown by the yellow arrow; it indicates that both ice roughness and snow surface undulations gave rises to the depth variations.

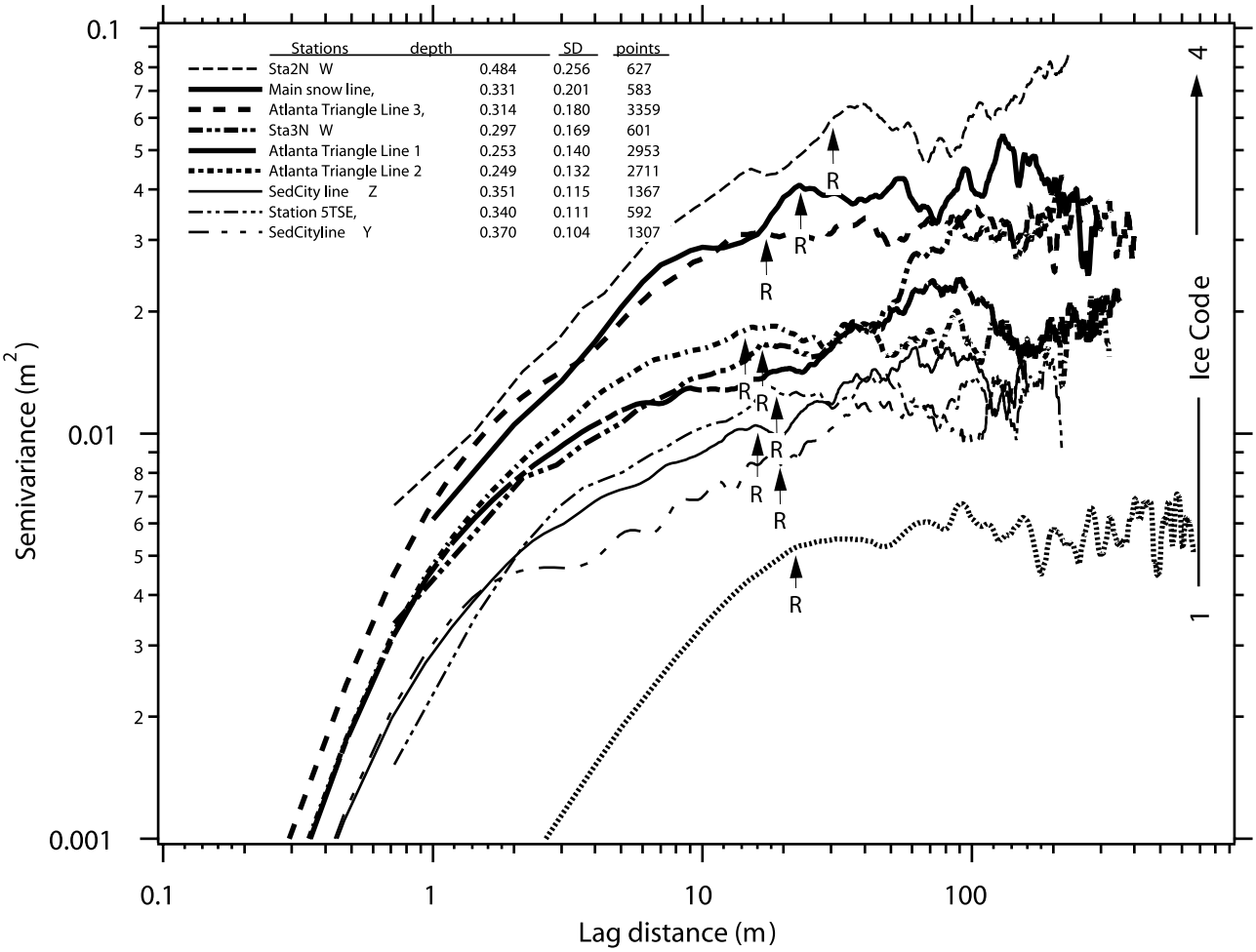


**Figure 12.** Semivariograms for snow depth for a wide variety of ice types. The "R" refers to the point on each curve where the semivariance reaches a sill value, which is known as the "range." This point defines the length scale of structures in the snow.

it describes the spatial variation in snow depth along a traverse line. The sill is a measure of the average amplitude, in this case the variation in snow depth, and it is approximately equal to $(SD)^2$. For lag intervals smaller than the range, the semivariance ($y$ values in Figure 12) increase monotonically because the sampling is within a coherent structure, but for lag distances greater than the range, the semivariance approaches a fixed value, which at SHEBA varied with ice class. The most interesting point is that for the snow at SHEBA the range ("R" in Figure 12) was nearly constant over a wide range of snow depths, ice types, and semivariances.

[29] One useful consequence of this 20 m patch finding is that for scale distances greater than 20 the snow depth at SHEBA behaved like random variable with a "regionalized" mean value set by ice class. As expected from Figure 10, the sill increased with increasing mean depth and SD of depth (see key on Figure 12). This systematic variation can also be expressed in terms of ice classes: As the ice got rougher (or as the ice class increased from 1 to 4), the semivariograms shifted upward, and perhaps just a little to the right. Semivariograms that intersected multiple ice ridges had the highest sills, while semivariograms with the lowest sills came from smooth floes of ice class 2 (no long lines were measured on ice class 1).

[30] We do not know the origin of the 20 m snow patch size, but we think it must have been the result of a complex interaction between ice roughness and the surface processes that create snowdrift features like dunes, barchans, and sastrugi [*Doumani*, 1966]. We note that semivariograms computed for stations with virtually flat ice (i.e., station 1 north) had snow surface undulations that averaged only 10 m in size, while ice ridges, acting like snow fences, created drift aprons that averaged about 25 m in width in each direction, for a bidirectional width of 50 m. From these data we conclude that neither the ridges nor the snowdrifts alone were the source of the 20 m patches. Yet when colocated snow and ice profiles are compared, an inverse linkage between the two is apparent. Snow surface elevation and ice features like melt pond edges and hummocks align. For example, in the cross section in Figure 11, a number of prominent high points at the snow surface appear directly above small refrozen melt pond depressions in the ice, and this visual impression is confirmed by the cross-correlation coefficient ($r = -0.57$ at a lag of 0.25 m). At station Delaware the cross-correlation coefficient ($r$) between snow

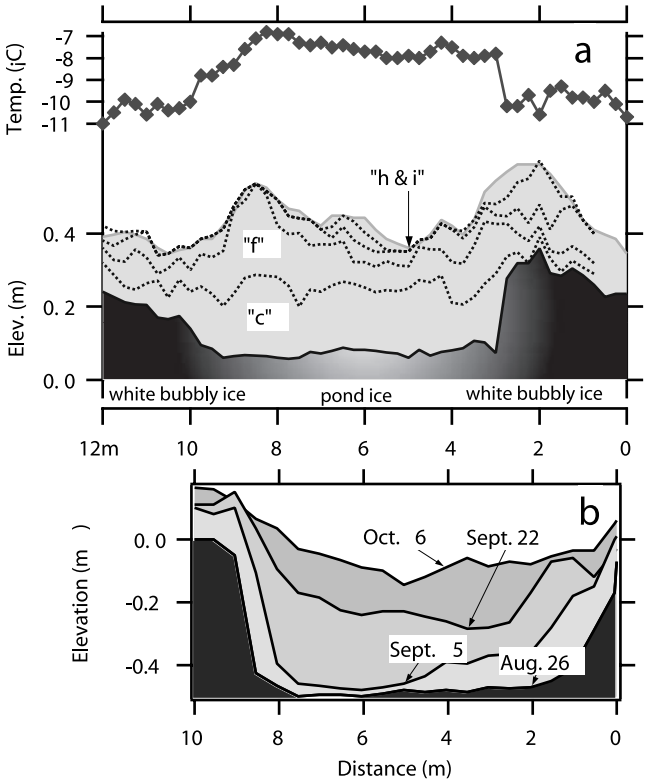


**Figure 13.** (a) Variations in snow properties across a small refrozen melt pond with the associated temperature of the snow-ice interface. (b) Sequence of snow filling a refrozen melt pond similar in size and shape to the one shown in Figure 13a, SHEBA camp, autumn of 1998.

surface peaks and melt pond depressions was −0.61. In both cases the snow depth structure length was about 20 m, while the ice structure length (structures other than ridges) was only about 10 m. These examples show that small and ubiquitous ice structures like melt pond edges nucleate snow features of longer wavelength, and these features persist, and are perhaps even enhanced, through multiple snowfall events like those that deposited the *f* and *g* slabs.

[31] These small-scale interactions between the ice and snow can feedback to ice growth, as the detailed cross section in Figure 13 suggests. The low edges (0.3 m) of a refrozen melt pond, interacting with drifting snow, have produced large lateral variations in the snow depth and stratigraphy (Figure 13a). Above the pond, snow layers *c* and *f* are considerably thicker than elsewhere, and slab layer *f* has created a dune that has subsequently helped to trap newer layers of snow. Adjacent to the pond, layer *b* is missing, but it is present as a thin layer over the pond (but not shown in Figure 13a for simplicity). In all, the pond depression is associated with a thicker snowpack containing more layers. Observations made in the closing days of the SHEBA experiment (Figure 13b) help explain how this depth enhancement over the pond might have occurred. During the ephemeral and rapid buildup stages of the winter of 1998–1999, wind transport of snow rapidly filled a melt pond depression similar to the one shown in Figure 13a. By early October the refrozen pond was already filled completely, while adjacent areas had been nearly swept clean of snow. This is also the reason that the snow at the sonic sounder located over the small melt pond at Seattle (Figure 2) showed deeper snow than on the nearby main line. This early season in-filling then created a favorable location for the trapping of drift snow during the remainder of the "buildup" and during the "winter storm" stages of the winter.

[32] This small-scale interaction between the snow and ice not only produced snow above ponds that was thicker, but it also ensured that the snow was in place earlier in the winter, a circumstance conducive to the development of depth hoar (Figure 6). Field observations confirmed that the depth hoar above small melt ponds was not only thicker, but was also less dense, more poorly bonded, and a better insulator than elsewhere. As a result, snow-ice interface temperatures tended to be higher (about 4° in the case illustrated in Figure 13a) above the ponds. Observations (H. Eicken, personal communication, 1999) suggest that the ice beneath such ponds is thinner than elsewhere, even in spring before albedo contrasts can account for the ice thickness differences. Indeed, during the winter at SHEBA, the ice over a refrozen melt pond at Seattle thickened from 0.9 to 1.4 m, while the hummocky ice at Quebec increased from 1.8 to 2.5 m; the initial thickness of the hummocky ice was twice that of the melt pond, yet there was 50% more ice growth. This difference was in large part due to the deeper, more insulative snow over the pond (40–60 cm) than over the hummocky ice (10–20 cm). We speculate that because of rapid early winter covering of refrozen melt ponds by snow, and the fact that this snow tends to retard the ice growth during the winter, the ponds will be thinner and tend to melt more readily in spring and therefore are more likely to become ponds again the following summer.

## 4. Discussion

[33] Are the snow measurements from SHEBA typical of the Arctic Basin in general? The average end-of-winter depth (33.7 cm) is nearly identical to tabulated and mapped values for the same sector of the Arctic based on measurements collected between 1954 and 1991 [*Radionov et al.*, 1997; *Warren et al.*, 1999]. The average density (0.343 g $cm^{-3}$) is slightly higher than the mapped value for the SHEBA area (0.330 g $cm^{-3}$ from the map of *Warren et al.* [1999]), but well within the scatter of the historical data. The combined depth and density for SHEBA give a mean SWE of 11.6 cm, which is close to the mean value for the entire basin of 11 cm. Moreover, across a large area of the central Arctic Basin the maps based on a 37 year record indicate only a limited range of depth and density, within which the SHEBA results fall nicely. Based on this comparison, we infer that the 1997–1998 snow cover at SHEBA was normal, unlike the ice under it, which was unusually thin [*Perovich et al.*, 2002]. We also suggest that the snow observed at SHEBA was representative of the snow cover over a wide areas of the central Arctic Ocean, perhaps excluding the eastern Arctic Basin, where winter precipitation rates and snow depths tend to be higher [*Serreze et al.*, 1997]. Unfortunately, we have been unable to find any detailed observations of snow stratigraphy against which to compare our stratigraphic results.

[34] The temporal evolution of the SHEBA snow cover also followed a pattern that appears to be typical. A rapid

build up of the snow cover from September through November, followed by a much lower rate of buildup between December and May, has been noted for the Arctic Basin in general by *Warren et al.* [1999], and the SHEBA results agree well with this pattern. By 11 October, there was already an average of about 11 cm of snow on the ice (Figures 2 and 4), and by 1 November the 15 cm values that match well with the results presented by *Warren et al.* [1999; Figure 13]. More specifically, the general increase of snow depth with time at SHEBA (Figure 2) is remarkably similar to results from drifting station A (1957–1958) as reported by *Untersteiner* [1961] and AIDJEX as reported by *Hanson* [1980], both of which were also located in the Beaufort Sea.

[35] The snow stratigraphy, which gave the snowpack its essential characteristics at SHEBA, was the product of a few limited wind and snow events, combined with the steady production of depth hoar due to strong temperature gradients imposed on the snow. Two additional questions need to be answered if we are to conclude the snow was typical: First, were temperature gradients unusually strong in 1997–1998, producing a greater amount of depth hoar than normal, and second, were the number of wind-slab-forming events unusually high or low?

[36] The answer to the first question is no. Air temperatures at SHEBA during 1997–1998 were slightly lower than normal during the winter but were slightly higher than normal in the spring [*Perovich et al.*, 1999a, 1999b], and the ice was thinner than normal (1.8 m instead of the more typical 2.5 m). Using a simple vertical, one-dimensional heat flow model in which we assume over periods of a month or more that the heat flow through the ice balanced the heat flow through the snow, we have computed the temperature gradients in the snow that that would have developed if the ice had been 3 m thick, and if "normal" temperatures (as indicated by *Martin and Munoz* [1997]) had prevailed. These calculated temperature gradients are about 20% lower than those observed (Figure 6) during the first four months of the winter, but are higher than observed in the spring. The 20% change is insufficient to drop the gradient below the critical value necessary for depth hoar formation, so we conclude that the change in depth hoar production would be negligible. Basically, the extremely low air temperatures and relatively high ice surface temperatures found throughout the Arctic Basin in winter ensure that depth hoar will develop every year, and it will always comprise a substantial amount (about 40%) of the snowpack, unless other factors (no snow or the snow is extremely dense slab) prevent its formation.

[37] Assessing whether the number of slab-forming winter storms was unusually high or low in 1997–1998 is more difficult. Analysis of the Comprehensive Ocean Atmosphere Data Set (COADS) [*Woodruff et al.*, 1987] by *Clark et al.* [1996] and *Serreze et al.* [1997] indicates that average surface wind speeds throughout the Arctic Basin are at, or below, the threshold necessary for snow transport (<5 m/s). In the COADS data the probability of high winds (in excess of 10 m/s) is greatest in September and October, drops in November through January, and then peaks again in February, but is never more than 6%. *Lindsay* [1998] obtained similar results using data from the Russian drifting stations. These results are consistent with the timing and the low number of winter storms observed at SHEBA, but since simultaneous wind and precipitation was necessary to produce the substantial slabs of 1997–1998, we really cannot tell if it was an unusual year or not. We want to emphasize again, however, how important these infrequent and short duration weather events can be in setting the characteristics of the snow cover in any given year.

## 5. Representing the Snow Cover in Ocean-Ice-Atmosphere Models

[38] In coupled ocean-ice-atmosphere models [*Maykut and Untersteiner*, 1971; *Ledley*, 1991; *Ebert and Curry*, 1993], snow cover is important because it insulates the ice, reducing the heat loss to the atmosphere during the winter, and also because it raises the albedo, increasing the amount of solar radiation reflected back to space. Snow depth and density, which are often specified, are used to determine many of the key snow properties of interest, like thermal conductivity. In many models, as snow depth increases, the layers of snow compact, and as they compact and increase in density, the value of thermal conductivity is increased since virtually all models use some variant of a positive density-thermal conductivity function [*Maykut and Untersteiner*, 1971; *Ledley*, 1991; *Ebert and Curry*, 1993; *Loth et al.*, 1993; *Lynch-Stieglitz*, 1994]. On the basis of our results we suggest the snow cover might best be modeled using the following approaches or approximations.

1. Temporal evolution of snow depth: The rapid buildup of the snow cover on the sea ice of the Arctic Basin that occurs in September, October and November has been described before [*Vowinkel and Orvig*, 1970; *Radionov et al.*, 1997; *Warren et al.*, 1999], and our data (Figure 2) show the same pattern. The timing and number of these early winter storms, and the amount of snow they deposit, is critical in determining the thermal history of the ice. Early storms will insulate the ice from the low air temperatures in November and December, and can therefore retard the growth of ice significantly. In the case of SHEBA the insulating blanket of the snow had nearly reached its maximum depth by mid-December. Failure to increase the snow depth early in model runs could lead to overestimates of early season heat losses. The rapid buildup can be modeled using published historical patterns, but we suggest it could also be modeled effectively using synoptic weather analyses. We note that in the case of SHEBA, only three or four events were needed to achieve the rapid build up.

[39] In a similar fashion, the limited number of weather events we have called "winter storms," responsible for the change in the snowpack during the remainder of the winter (Figures 4 and 5), are the result of specific and predictable synoptic events that could be modeled either stochastically or deterministically. The weather-to-snow layer connections are fairly simple: Small snowfalls rarely are preserved in the stratigraphic column (Figure 4), while the development of important layers of snow in the pack (such as *f*) require nearly simultaneous high wind and snowfall (Figure 5). The latter is a rare combination in any given winter, and therefore the likelihood of depositing several *f* slabs is not high. The limiting factor is precipitation, not wind, which is frequently strong enough to transport fresh snow, so the modeling problem comes down to accurately simulating

when (or if) large amounts of mid-winter precipitation will occur. We note that for the winter of 1997–1998, the entire snowpack was created during an aggregate of just 14 days out of a 240 day winter, or less than 6% of the total time. The motivation for modeling snow cover formation in this way is that a single weather event, for example the event that created the *f* slab, can have a profound impact on the depth distribution and thermal/mechanical properties of the snow cover.

2. Temporal evolution of snow density: Two of the three types of snow found in the pack (wind slab and depth hoar; Table 2 and Figure 3) resist densification. In addition, the thin snowpack at SHEBA, and the Arctic Basin in general, provides little overburden pressure to cause layers of snow to densify. Assuming an initial density for each snow layer, perhaps based on wind speed or precipitation rates, and then keeping the density of that layer constant through the remainder of the winter, may be the most accurate way to represent the snow cover evolution. On the basis of 37 years of data, *Radionov et al.* [1997] noted little change in the bulk density of the Arctic Basin snowpack between December and April, consistent with the approach we are suggesting.

3. Depth hoar formation: Depth hoar is an excellent insulator and results in low bulk values of thermal conductivity for the snow cover [*Sturm and Johnson*, 1992; *Sturm et al.*, 1997]. We have shown (Figure 6) and discussed why depth hoar will form reliably, rapidly and continuously on the sea ice each winter. *Fukuzawa and Akitaya* [1993] have published rates of depth hoar formation versus temperature gradients in the snow, and *Akitaya* [1974] has observed that high-density layers like wind slabs will resist metamorphosing into depth hoar. Snow temperature gradients can be readily estimated in models, and wind speeds can be used to determine if a layer has been deposited at a density too high to allow metamorphosis. Allowing snow layers to evolve into depth hoar in models might produce more accurate estimates to the bulk thermal conductivity.

4. Wind slab formation: The air layer immediately above the snow surface on Arctic sea ice is frequently supersaturated with water vapor [*Andreas et al.*, 2002], due in large part to moisture available from abundant leads. Surface riming and hoarfrost formation may increase the bonding in surface snow layers and therefore decrease the likelihood of wind drifting after deposition. This characteristic makes it even more likely that combined snow and wind events are needed to produce robust slab layers in the snowpack of the Arctic Basin, and could further simplify modeling of the snow cover (by removing the need to model drifting after deposition). However, the phenomenon needs to be better documented before implemented in models.

5. Variation of snow characteristics by ice class: Snow depth can be tied to ice class (Figure 10 and Table 3). If the ice class can be determined by remote sensing, then the spatial distribution of depth can be modeled over large areas. In addition to depth, the SD of depth, the SWE, the number of snow layers, and the amount of wind slab and depth hoar all seemed to vary by ice class (Table 3; Figures 9 and 10). Using even simple ice-to-snow relationships should result in an improvement in the accuracy of representing this wide range of snow characteristic in simulations. We chose four classes of ice, but our central two classes could rarely be differentiated. Perhaps three classes of ice (thin, deformed, and undeformed) would be sufficient for the purposes of simulating the snow cover.

6. Modeling snowdrifts associated with ice ridges: Drifting snow creates wedge-shaped aprons of snow about 25 m wide that blanket both flanks of ice ridges. While these drifts are fairly conspicuous, our measurements indicate that their relative volume is small: they occupy less than 6% of the total ice surface area and averaged over their whole width are only about 30% deeper than normal snow. However, the drifts play an important thermal role that has biological consequences. The drifts are thickest, and therefore reduce the heat flow the most, exactly above the cracks in the ice that parallel the ridges. As a consequence, these seawater filled cracks can and often do remain unfrozen throughout the winter (to the peril of a traveler). Seals use the cracks for access to the ice surface and den in the drifts. Modeling of the drifts may not be important from the standpoint of mass balance, but may be necessary to predict heat losses and changes of climate and ice conditions on the marine mammals.

7. Small-scale processes and depth distribution within ice classes: Snow depth varied at the surprisingly reliably length scale of 20 m (Figure 12), regardless of ice class. This small-scale variation is well below the grid scale of most models, which is convenient because at scales greater than 20 m, the depth can be treated like a normally distributed random variable with the mean and SD set by ice type (Figures 9 and 12). Caution needs to be exercised, however, because variations in snow depth, density, and character at scales of 1–20 m can be large, and the characteristics and evolution of the snowpack can vary sharply over these short distances. This lateral variability gives rise to variations in temperatures that are surprisingly large (Figure 13). In particular, there appears a close association between these small-scale variations and melt pond features, which are ubiquitous over the ice. Over melt ponds the snow is not only deeper, but forms much earlier in the season than elsewhere, a process that could have important implications for the production of ice during the winter.

[40] **Acknowledgments.** We thank the crew of the Canadian Coast Guard icebreaker *Des Groseilliers* along with logistics group from the University of Washington Applied Physics Laboratory for their superb support during the SHEBA field program. B. Elder, J. Richter-Menge, W. B. Tucker III, T. Udall, H. Eiken, T. Grenfell, and B. Light assisted in collecting snow measurements. We thank R. E. Moritz and the staff of the SHEBA Project Office for providing us with meteorological data. This work was funded as part of the SHEBA program by the Office of Naval Research High Latitude Physics Program and the National Science Foundation Arctic System Science Program.

## References

Akitaya, E., Studies on depth hoar, *Contrib. Inst. Low Temp. Sci., Ser. A*, *26*, 1–67, 1974.

Andreas, E. L., P. S. Guest, P. O. G. Persson, C. W. Fairall, T. W. Horst, R. E. Moritz, and S. R. Semmer, Near-surface water vapor over polar sea ice is always near ice-saturation, *J. Geophys. Res.*, *107*, 8033, doi:10.1029/2000JC000411, 2002.

Armstrong, R. L., An analysis of compressive ctrain in adjacent temperature-gradient and equi-temperature layers in a natural snow cover, *J. Glaciol.*, *26*, 283–289, 1980.

Armstrong, R. L., Metamorphism in a subfreezing, seasonal snow cover: The role of thermal and vapor pressure conditions, Ph.D. thesis, Univ. of Colo., Boulder, 1985.

Barry, R. G., The parameterization of surface albedo for sea ice and its snow cover, *Prog. Phys. Geogr.*, *20*, 63–79, 1996.

Benson, C. S., Reassessment of winter precipitation on Alaska's Arctic slope and measurements on the flux of wind blown snow, *Rep. UAG R-288*, 26 pp., Geophys. Inst., Univ. of Alaska, Fairbanks, 1982.

Birkeland, K. W., Terminology and predominant processes associated with the formation of weak layers of near-surface facted crystals in the mountain snowpack, *Arct. Alp. Res.*, *30*, 193–199, 1998.

Black, R. F., Precipitation at Barrow, Alaska, greater than recorded, *Eos Trans. AGU*, *35*, 203–206, 1954.

Clark, I., The semivariogram, in *Geostatistics*, edited by A. Royle et al., pp. 17–40, McGraw-Hill, New York, 1980.

Clark, M. P., M. C. Serreze, and R. G. Barry, Characteristics of Arctic Ocean climate based on COADS data, 1980–1993, *Geophys. Res. Lett.*, *23*, 1953–1956, 1996.

Colbeck, S., E. Akitaya, R. Armstrong, H. Gubler, J. Lafeuille, K. Lied, D. McClung, and E. Morris, The international classification for seasonal snow on the ground, *Rep. MP 2794*, 23 pp., Int. Comm. on Snow and Ice, Int. Assoc. of Sci. Hydrol., Gentbrugge, Belgium, 1992.

Davis, J. C., *Statistics and Data Analysis in Geology*, 646 pp., John Wiley, New York, 1986.

Doumani, G. A., Surface structures in snow, in *International Conference on Low Temperature Science*, vol. 1, *Physics of Snow and Ice*, pp. 1119–1136, Hokkaido Univ., Hokkaido, Japan, 1966.

Ebert, E. E., and J. A. Curry, An intermediate one-dimensional thermodynamic sea ice model for investigating ice-atmosphere interactions, *J. Geophys. Res.*, *98*, 10,085–10,109, 1993.

Fukuzawa, T., and E. Akitaya, Depth-hoar crystal growth in the surface layer under high temperature gradient, *Ann. Glaciol.*, *18*, 39–45, 1993.

Geiger, R., *The Climate Near the Ground*, 494 pp., Harvard Univ. Press, Cambridge, Mass., 1957.

Goodison, B. E., and D. Yang, In-situ measurement of solid precipitation in high latitudes: The need for correction, paper presented at Workshop on the ACSYS Solid Precipitation Climatology Project, World Meteorol. Org., Geneva, 1996.

Goodison, B. E., H. L. Ferguson, and G. A. McKay, Measurement and data analysis, in *Handbook of Snow*, edited by D.M. Gray and D. H. Male, pp. 191–274, Pergamon, New York, 1981.

Hanson, A. M., The snow cover of sea ice during the Arctic Ice Dynamics Joint Experiment, 1975–1976, *Arc. Alp. Res.*, *12*, 215–226, 1980.

Holmgren, J., M. Sturm, N. E. Yankielun, and G. Koh, Extensive measurements of snow depth using FM-CW radar, *Cold Reg. Sci. Technol.*, *27*, 17–30, 1998.

Isaaks, E. H., and R. M. Srivastava, *An Introduction to Applied Geostatistics*, 561 pp., Oxford Univ. Press, New York, 1989.

Kuz'min, P. P., Snow cover and snow reserves, 140 pp., Isr. Prog. for Sci. Transl., Off. of Tech. Serv., U.S. Dept. of Commerce, Washington, D.C., 1963.

Ledley, T. S., Snow on sea ice: Competing effects in shaping climate, *J. Geophys. Res.*, *96*, 17,195–17,208, 1991.

Lindsay, R. W., Temporal variability of the energy balance of thick Arctic pack ice, *J. Clim.*, *11*, 313–333, 1998.

Loth, B., H. F. Graf, and J. M. Oberhuber, Snow cover model for global climate simulations, *J. Geophys. Res.*, *98*, 10,451–10,464, 1993.

Lynch-Stieglitz, M., The development and validation of a simple snow model for the GISS GCM, *J. Clim.*, *7*, 1842–1855, 1994.

Magono, C., and C. W. Lee, Meteorological classification of natural snow crystals, *J. Fac. Sci. Hokkaido Univ., Ser.*, *2*, 321–335, 1966.

Marbouty, D., An experimental study of temperature-gradient metamorphism, *J. Glaciol.*, *26*, 303–312, 1980.

Martin, S., and E. A. Munoz, Properties of the Arctic 2-m air temperature for 1979-present derived from a new gridded data set, *J. Clim.*, *10*, 1428–1440, 1997.

Maykut, G. A., and N. Untersteiner, Some results from a time-dependent thermodynamic model of sea ice, *J. Geophys. Res.*, *76*, 1550–1575, 1971.

Mellor, M., Properties of snow, *Rep. III-A1*, U.S. Army Cold Reg. Res. and Eng. Lab., Hanover, N.H., 1964.

Nakaya, U., *Snow Crystals, Natural and Artificial*, 510 pp., Harvard Univ. Press, Cambridge, Mass., 1954.

Nyberg, A., Temperature measurements in an air layer very close to a snow surface, *Geogr. Ann.*, *16*, 237–275, 1938.

Perovich, D. K., and B. Elder, Temporal evolution and spatial variability of the temperature of Arctic sea ice, *Ann. Glaciol.*, *33*, 207–211, 2001.

Perovich, D. K., et al., Year on ice gives climate insights, *Eos Trans. AGU*, *80*, 481, 1999a.

Perovich, D. K., T. C. Grenfell, B. Light, J. A. Richter-Menge, M. Sturm, W. B. Tucker III, H. Eicken, G. A. Maykut, *SHEBA: Snow and Ice Studies* [CD-ROM], U.S. Army Cold Reg. Res. and Eng. Lab., Hanover, N.H., 1999b.

Perovich, D. K., et al., Aerial observations of the evolution of ice surface conditions during summer, *J. Geophys. Res.*, *107*, doi:10.1029/2000JD000449, in press, 2002.

Pomeroy, J. W., and D. M. Gray, Snow cover accumulation, relocation and management, *NHRI Sci. Rep. 7*, 134 pp., Nat. Hydrol. Res. Inst., Saskatoon, Sask., Canada, 1995.

Radionov, V. F., N. N. Bryazgin, and E. I. Alexandrov, The snow cover of the Arctic basin, *Rep. APL-UW-TR 9701*, Appl. Phys. Lab., Univ. of Wash., Seattle, Wash., 1997.

Seligman, G., *Snow Structure and Ski Fields*, 555 pp., Int. Glaciol. Soc., Cambridge, Mass., 1980.

Serreze, M. C., J. A. Maslanik, and J. R. Key, Atmospheric and sea ice characteristics of the Arctic Ocean and the SHEBA field region in the Beaufort Sea, *Rep. 4*, 217 pp., Nat. Snow and Ice Data Cent., Coop. Inst. for Res. in Environ. Sci., Boulder, Colo., 1997.

Sturm, M., The role of thermal convection in heat and mass transport in the subarctic snow cover, *Rep.* 91-19, U.S. Army Cold Reg. Res. and Eng. Lab., Hanover, N.H., 1991.

Sturm, M., and C. S. Benson, Vapor transport, grain growth and depth hoar development in the subarctic snow, *J. Glaciol.*, *43*, 42–59, 1997.

Sturm, M., and J. Holmgren, Differences in compaction behavior of three climate classes of snow, *Ann. Glaciol.*, *26*, 125–130, 1998.

Sturm, M., and J. B. Johnson, Thermal conductivity measurements of depth hoar, *J. Geophys. Res.*, *97*, 2129–2139, 1992.

Sturm, M., J. Holmgren, M. König, and K. Morris, The thermal conductivity of seasonal snow, *J. Glaciol.*, *43*, 26–41, 1997.

Sturm, M., K. Morris, and R. Massom, The winter snow cover of the West Antarctic pack ice: Its spatial and temporal variability, in *Antarctic Sea Ice: Physical Processes, Interactions and Variability, Ant. Res. Ser.*, vol. 74, edited by M. O. Jeffries, pp. 1–18, AGU, Washington, D.C., 1998.

SYSTAT, *Statisitics Software Manual*, SYSTAT Inc., Evanston, Ill., 1989.

Takeuchi, M., Vertical profile and horizontal increase of drift-snow transport, *J. Glaciol.*, *26*, 481–492, 1980.

Trabant, D., and C. S. Benson, Field experiments on the development of depth hoar, *Geol. Soc. Am. Mem.*, *135*, 309–322, 1972.

Untersteiner, N., On the mass and heat budget of Arctic sea ice, *Arch. Meteorol. Geophys. Bioklimatol., Ser. A*, *12*, 151–182, 1961.

von Eugster, H. P., On the form and metamorphosis of snow, *Rep. 113*, Inst. for Snow and Avalance Res., Davos, Switzerland, 1950.

Vowinckel, E., and S. Orvig, The climate of the north polar basin, in *Climates of the Polar Regions-World Survey of Climatology*, edited by S. Orvig, pp. 129–252, Elsevier Sci., New York, 1970.

Warren, S. G., I. G. Rigor, N. Untersteiner, V. F. Radionov, N. N. Bryazgin, Y. I. Aleksandrov, and R. Colony, Snow depth on arctic sea ice, *J. Clim.*, *12*, 1814–1829, 1999.

Woodruff, S. D., R. J. Slutz, R. L. Jenne, and P. M. Steurer, A comprehensive ocean-atmosphere data set, *Bull. Am. Meteorol. Soc.*, *68*, 1239–1250, 1987.

---

J. Holmgren and M. Sturm, U.S. Army Cold Regions Research and Engineering Laboratory–Alaska, P.O. Box 35170, Ft. Wainwright, AK 99703-0170, USA. (holmgren@crrel.usace.army.mil; msturm@arrel.usace.army.mil)

D. K. Perovich, U.S. Army Cold Regions Research and Engineering Laboratory, 72 Lyme Road, Hanover, NH 03755-1290, USA. (perovich@crrel.usace.army.mil)